Technical Report

TR-14-25

Buffer homogenisation, status report 2

Ann Dueck, Reza Goudarzi, Lennart Börgesson
Clay Technology AB

December 2014

Svensk Kärnbränslehantering AB
Swedish Nuclear Fuel
and Waste Management Co

Box 250, SE-101 24 Stockholm
Phone +46 8 459 84 00

ISSN 1404-0344
SKB TR-14-25
ID 1432128

Buffer homogenisation, status report 2

Ann Dueck, Reza Goudarzi, Lennart Börgesson
Clay Technology AB

December 2014

Keywords: Bentonite, Swelling, Swelling pressure, Homogenisation.

Abstract

The present status report is a compilation of laboratory test results from homogenisation tests on a Wyoming bentonite. The main purpose of the status report is to provide results that can be used for modelling some well-defined benchmark tests in order to improve the models or determine mechanical parameters for thermo-hydro-mechanical modelling of the behaviour of the buffer.

Results from fundamental laboratory tests and from a laboratory study of the influence of friction are presented.

Sammanfattning

Denna lägesrapport innehåller en sammanställning av laboratorieförsök som utförts för att studera homogeniseringsprocessen hos buffertmaterial. Huvudsyftet med rapporten är att tillhandahålla resultat som kan användas för modellering av några väldefinierade prestandatester för att förbättra modellerna eller för att bestämma mekaniska parametrar för den termo-hydro-mekaniska modelleringen av buffertens uppförande.

Resultatet från grundläggande laboratorieförsök och från en studie av inverkan av friktion presenteras.

Contents

1 Introduction

1.1 Background

Swelling of the buffer blocks and buffer homogenisation are important functions to guarantee the fulfilment of requirements set for the buffer after full water saturation. It is important to understand and predict the final condition of the buffer after the swelling and homogenisation, which occurs both during the initial saturation and after a possible loss of bentonite caused by for example erosion.

Simplified material models have previously been used in the analyses of homogenisation processes. However, there are uncertainties in the models and the models need to be checked and improved, if necessary.

The project consists of four parts; theoretical studies, fundamental laboratory tests, laboratory study of the influence of friction and large scale tests of the case involving loss of bentonite. The present status report describes results from fundamental laboratory tests and from the study of influence of friction.

The tests described were run during 2011 and January 2012. This second status report is a continuation of the previous status report (Dueck et al. 2011) where results from 2009–2010 were presented.

1.2 Objective

The objective of the described tests has been to further improve the knowledge of the process of swelling and buffer homogenisation. The main purpose of this status report is to provide results that can be used for modelling some well-defined benchmark tests in order to improve the models or determine mechanical parameters for thermo-hydro-mechanical modelling of the behaviour of the buffer.

1.3 Comments on performed tests

Some of the tests run in this project were used as tasks in the project EBS-TF. Results from tests A01-9, A01-10, R11-18, R11-19, R21-9 and R21-10 were used as tasks but in EBS-TF the labels A1, A2, Ro1, Ro2, Ri1 and Ri2, were used. In addition, results from tests A01-12, A01-13, R21-11 and R21-12 were presented to the project EBS-TF as background data. The results from the so called high resolution series and the tests on friction between buffer and other surfaces were also presented as background data within the referred project.

In a few cases (during the actual test period only one case) dismantled specimens were found to be clearly unsaturated. Such results are disregarded and not further interpreted.

The specimens used in this report were all supplied with de-ionized water during saturation and the subsequent homogenisation and as long as nothing else is specified the water was stagnant.

2 Determination of basic variables

2.1 General

From each test the basic variables water content and bulk density are measured and from those variables the dry density and degree of saturation are calculated. During each test the radial and axial swelling pressures are measured.

2.2 Water content and bulk density determination

The basic geotechnical variables water content w (%), void ratio e, degree of saturation S_r (%) and dry density ρ_d (kg/m^3) are determined according to Equations 2-1 to 2-4.

$$w = 100 \cdot \frac{m_{tot} - m_s}{m_s} \qquad \text{(Equation 2-1)}$$

$$e = \frac{\rho_s}{\rho}(1 + w/100) - 1 \qquad \text{(Equation 2-2)}$$

$$S_r = \frac{\rho_s \cdot w}{\rho_w \cdot e} \qquad \text{(Equation 2-3)}$$

$$\rho_d = \frac{m_s}{V} \qquad \text{(Equation 2-4)}$$

where

m_{tot} = total mass of the specimen (kg)

m_s = dry mass of the specimen (kg)

ρ_s = particle density (kg/m^3)

ρ_w = density of water (kg/m^3)

ρ = bulk density of the specimen (kg/m^3)

V = total volume of the specimen (m^3)

The water content is defined as the ratio between the mass of water and the dry mass of a specimen according to Equation 2-1. The dry mass of a specimen is obtained from drying a wet specimen at 105˚C for 24h. The bulk density is calculated from the total mass of a specimen and the volume determined by weighing the specimen above and submerged into paraffin oil.

2.3 Swelling pressure determination

The swelling pressure is determined as axial and radial stresses exerted as loads on a piston with a certain area.

3 Material

The material used in the test series is the commercial Wyoming bentonite with brand name Volclay MX-80 from American Coll. Co. The powder used for the actual tests was delivered before 2010. The powder was delivered with an approximate water content of 10%. For tests where higher initial water content was needed the powder was mixed with de-ionized water. Specimens made by compacted powder were used in the test series and some specimens were compacted directly to the size needed and some were sawn from larger compacted blocks.

For determination of void ratio and degree of saturation the particle density ρ_s = 2,780 kg/m^3 and water density ρ_w = 1,000 kg/m^3 have been used.

4 Test technique

4.1 Fundamental swelling tests – basic series

Swelling of water saturated bentonite specimens with access to water was studied in three test series. The principle is illustrated in Figure 4-1:

- Axial swelling in a device with constant radius and limited height. Variation of the height of the gap. (A0).
- Radial swelling of the outer surface in a device with constant height and limited radius. Variation of the radial gap. (R1).
- Radial swelling into a cylindrical cavity in a device with constant height and radius. Variation of the radius of the cavity. (R2).

The tests were mainly done with free swelling surfaces, i.e. no counteracting force until the swelling bentonite gel had reached the outer limited surface. In all tests the friction was minimized by use of a mineral-oil based lubricant on relevant surfaces.

Equipment

The three different types of test were carried out in devices with the design shown in Figure 4-2 to Figure 4-4. The equipment consists of a steel ring surrounding each specimen. In the device used for axial swelling a filter is placed above the specimen, which covers the cross section area. In case of the radial swelling a circular radial filter is placed between the circumference of the specimens and the steel ring. In all three types of test the top and bottom plates are bolted together with the steel ring to keep the volume constant. In each set-up two load cells are placed in the vertical and radial direction, respectively. In all three types of test the load cells used for radial measurements are placed at a level corresponding to half of the initial height of the specimens. The load cells are placed between a fixed plate and a movable piston where small deformation required by the load cells is admitted. During the entire course of the tests the forces were measured by the load cells which were calibrated prior to, and checked after, each test.

Preparation of specimens

Cylindrical specimens were prepared by compaction of powder to a certain density. The specimens used for the axial type of swelling had a diameter of 50 mm and a height of 20 mm. For the radial types of swelling specimens with diameter 47 mm and height 40 mm were used.

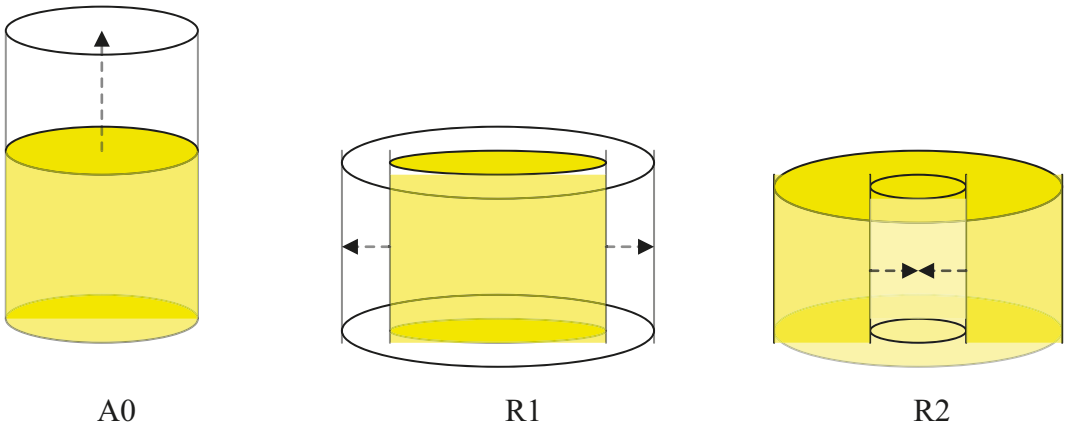

Figure 4-1. *Illustration of the geometry of the test types carried out.*

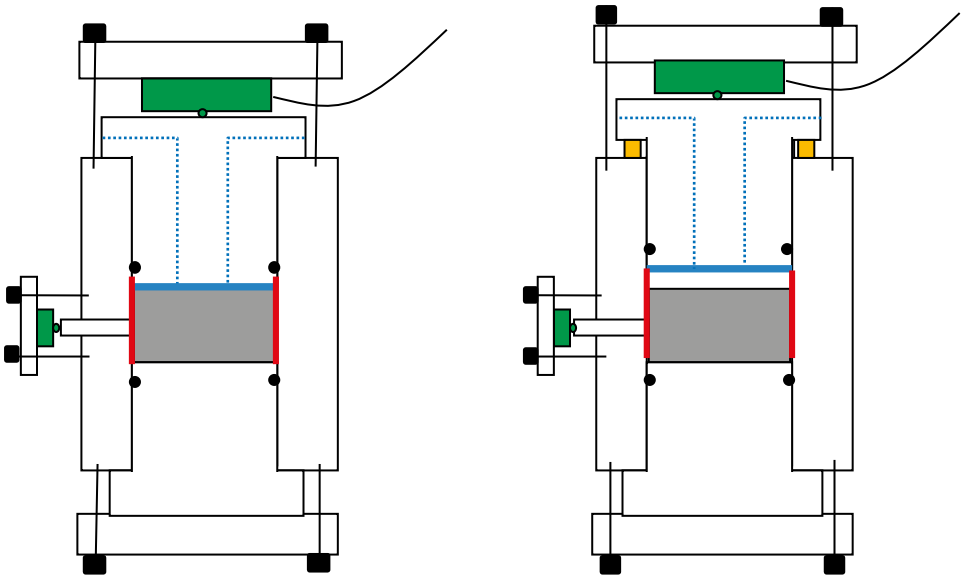

Figure 4-2. *Set-up used for the axial swelling tests (A). The red lines represent the lubricated surfaces and the blue lines represent filters and water supply.*

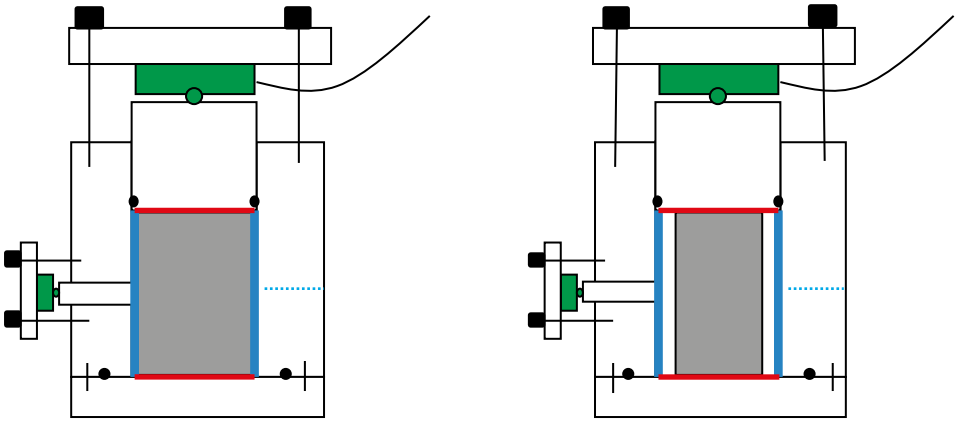

Figure 4-3. *Set-up used for the radial outward swelling tests (R1). The red lines represent the lubricated surfaces and the blue lines represent filters and water supply.*

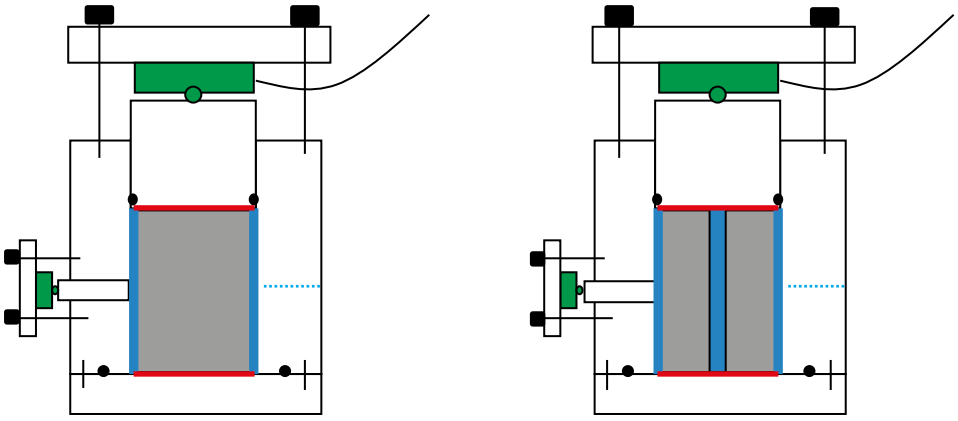

Figure 4-4. *Set-up used for the inward radial swelling tests (R2). The red lines represent the lubricated surfaces and the blue lines represent filters and water supply.*

Test procedure

The tests consisted of two phases; the water saturation phase and the swelling phase. The swelling phase included both the relatively large swelling and the homogenisation. After mounting the specimen in one of the devices shown in Figure 4-2 to Figure 4-4, de-ionized water was applied to the filters after air evacuation of the filters and tubes. The specimens had free access to water during the water saturation. When only small changes in swelling pressure with time were noticed the water was evacuated from the filters and tubes and the second phase, i.e. the swelling, started. Depending on the type of swelling the following measures were taken;

- For the axial swelling (A0) the upper piston was moved upwards and fixed with spacers admitting a certain volume for the swelling. After evacuation of air, water was applied to the upper part of the specimen.
- For the radial swelling of the outer surface (R1) the water-saturated specimen was taken out and the diameter decreased by trimming the circumference of the specimen leaving a certain volume for swelling after re-mounting it in the same device. After evacuation of air the filter was filled with water.
- For the radial swelling of an inner cavity (R2) the lower lid was opened and a hole was drilled in the center of the specimen. The cavity was filled with water, the lid was fixed and the outer filter was filled with water after evacuation of air.

After completed swelling and homogenisation, i.e. when no or negligibly small changes were noticed in the swelling pressure with time, the specimens were dismantled and cut in slices for determination of water content and density distribution in the direction of swelling.

Test results

The test results are presented with w, ρ_d and S_r as a function of the specimen height (series A0) or radius (series R1 and R2), i.e. as distribution in the direction of swelling. The measured stresses are also shown and compared with a model of swelling pressure presented by Börgesson et al. (1995). The swelling was calculated for all tests according to Equation 4-1 where V_i, V_f, ρ_{di} and ρ_{df} are the initial volume, final volume, initial dry density and final dry density, respectively.

$$s = \frac{\Delta V}{V_i} = \frac{V_f}{V_i} - 1 = \frac{\rho_{di}}{\rho_{df}} - 1 \qquad \text{(Equation 4-1)}$$

Test series

As described earlier three different types of swelling were studied; one type of axial swelling and two types of radial swelling. The axial swelling (A0) took place in the same direction as the compaction and the radial swelling (R1 and R2) took place perpendicular to the direction of compaction.

The original test series included swelling between 0 and approximately 30%. From an initial dry density of approximately 1,660 kg/m^3 the final dry density was approximately 1,270 kg/m^3 after 30% of swelling. The corresponding changes in height and diameter for each series are shown in Table 4-1.

Table 4-1. Examples of final dimensions of the specimens used in each type of swelling.

Test type	Swelling $\Delta V/V_0$ (%)	Final values of Height H (mm)	Final values of Diameter D (mm)	Change in ΔH (mm)	Change in circumferential ΔD_1 (mm)	Change in cavity ΔD_2 (mm)
Axial A0	0–30	20–26	50	0–6		
Radial R1	0–30	40	46.8		0–6	
Radial R2	0–30	40	46.8			0–23

4.2 Fundamental swelling tests – high resolution

In the High Resolution (HR) series the same type of tests as in the basic series were run. The main difference between the two series was the size of the specimens where the larger specimens in the HR-series admitted higher resolution in the distribution of base variables over the specimens.

As in the basic series swelling was studied in three series; axial swelling (HR-A), radial outward swelling (HR-Ro) and radial inward swelling (HR-Ri), illustrated in Figure 4-1. As in the basic series the tests were mainly done with free swelling surfaces, i.e. no counteracting force until the swelling bentonite gel had reached the outer limited surface. In all tests the friction was minimized by use of a mineral-oil based lubricant on relevant surfaces.

Equipment

The three different types of test were carried out in devices with the design shown in Figure 4-5 to Figure 4-7. The devices consist of a steel ring surrounding the specimen. A movable piston is placed vertically, in the axial direction above the specimen. Radial pistons are placed in holes through the steel ring for measurement of radial forces.

In the device used for the axial swelling a steel filter is placed on the upper side of the sample while in case of radial swelling a radial plastic filter is placed between the surrounding steel ring and the specimen.

In the devices the bottom and top plates and the steel ring are bolted together to keep the volume constant. Load cells are placed in the vertical and radial directions. The load cells are placed between a fixed plate and the movable piston where the small deformation required by the load cell is admitted. During the entire course of the tests the forces were measured by the load cells which were calibrated prior to, and checked after, each test.

Preparation of specimens

The specimens were sawn and trimmed from larger blocks with the initial water content 24% and the degree of saturation approximately 98%. The final height and diameter for the specimens swelling axially were 50 mm and 100 mm, respectively and for the specimens swelling radially the final height and diameter were 80 mm and 97 mm, respectively.

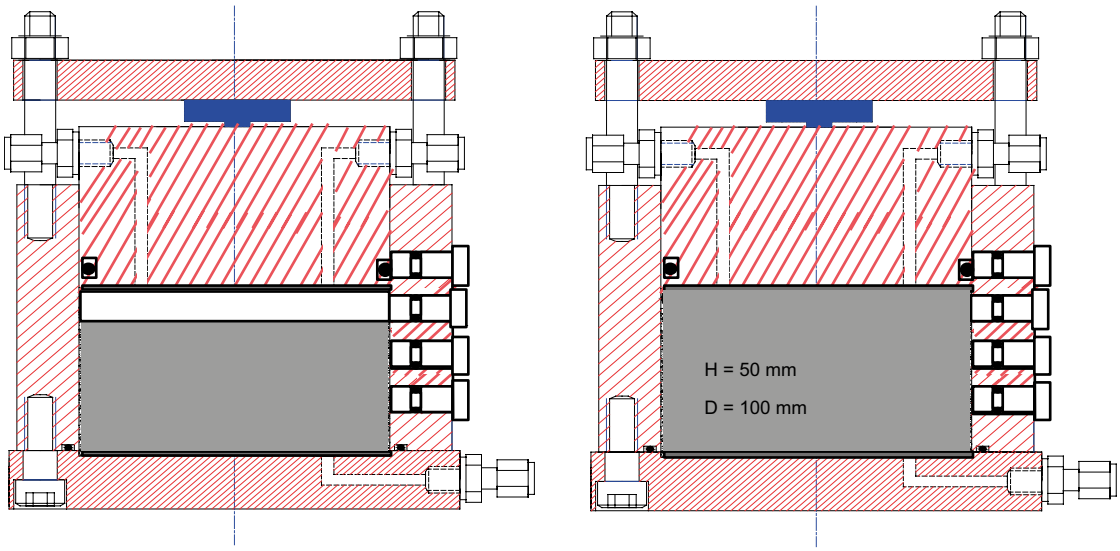

Figure 4-5. *Set-up used for the axial swelling tests (HR-A). Water was only supplied from a filter placed above the specimen.*

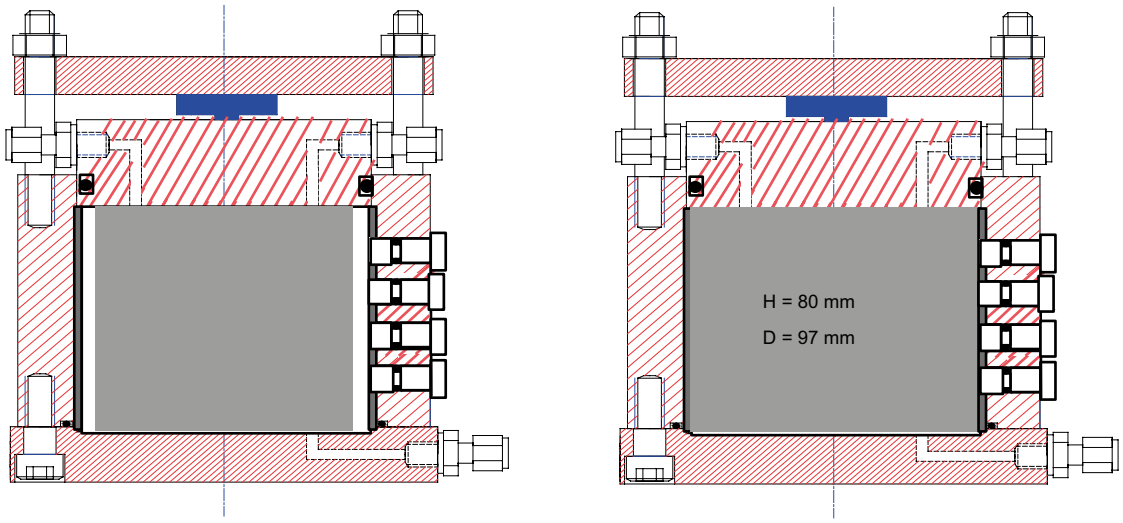

Figure 4-6. *Set-up used for the radial outward swelling tests (HR-Ro). Water was supplied from a radial filter between the surrounding steel ring and the specimen. The radial stress was generally only measured at one level.*

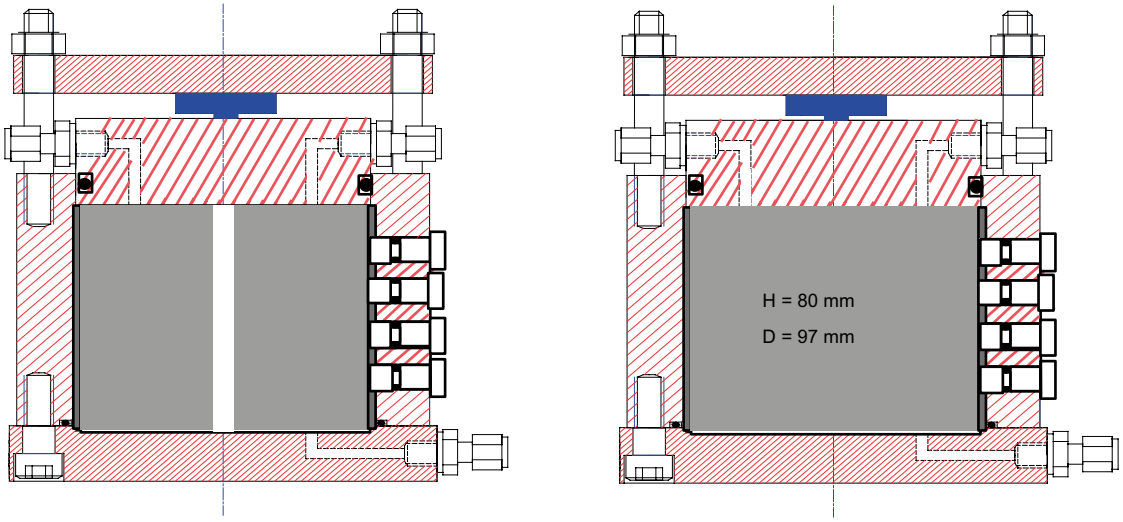

Figure 4-7. *Set-up used for the inward radial swelling tests (HR-Ri). Water was initially filled into the cavity and then only supplied from a radial filter between the surrounding steel ring and the specimen. The radial stress was generally only measured at one level.*

Test procedure

In the HR-series the initial degree of saturation was high to avoid the time consuming saturation phase and for that reason the swelling and homogenisation phase started directly. After preparation the specimens were mounted into one of the devices shown in Figure 4-5 to Figure 4-7 and de-ionized water was applied to the filters after air evacuation of the filters and tubes. In accordance with the fundamental tests in the basic series water was only applied to the upper part of the specimen at axial swelling, only applied to the radial filter at radial outward swelling and at the radial inward swelling applied to the radial filter and also filled into the cavity.

After completed swelling and homogenisation, i.e. when no or negligibly small changes were noticed in the measured swelling pressure, the specimens were dismantled and cut in slices for determination of water content and density distribution in the direction of swelling.

Test results

The test results are presented with w, ρ_d and S_r as a function of the specimen height (series HR-A) or radius (series HR-Ro and HR-Ri), i.e. as distribution in the direction of swelling. The measured stresses are also shown and compared with a model of swelling pressure presented by Börgesson et al. (1995) and test results presented by Karnland et al. (2006). The swelling was calculated according to Equation 4-1.

Test series

In the test series with different types of swelling, one type of axial swelling and two types of radial swelling, were run.

4.3 Measurements of friction between buffer and other surfaces

Friction between confined specimens at saturation and different types of surfaces was studied with a new test set-up.

Equipment

The tests were carried out in the device shown with a sketch in Figure 4-8. The swelling pressure device consists of a steel ring surrounding the specimen having filters on both sides. The inner surface of the ring can be prepared in different ways for example with or without lubrication. Two pistons are placed vertically, in the axial direction, above and below the specimen. A radial piston is placed in a hole through the steel ring for measurement of the radial pressure.

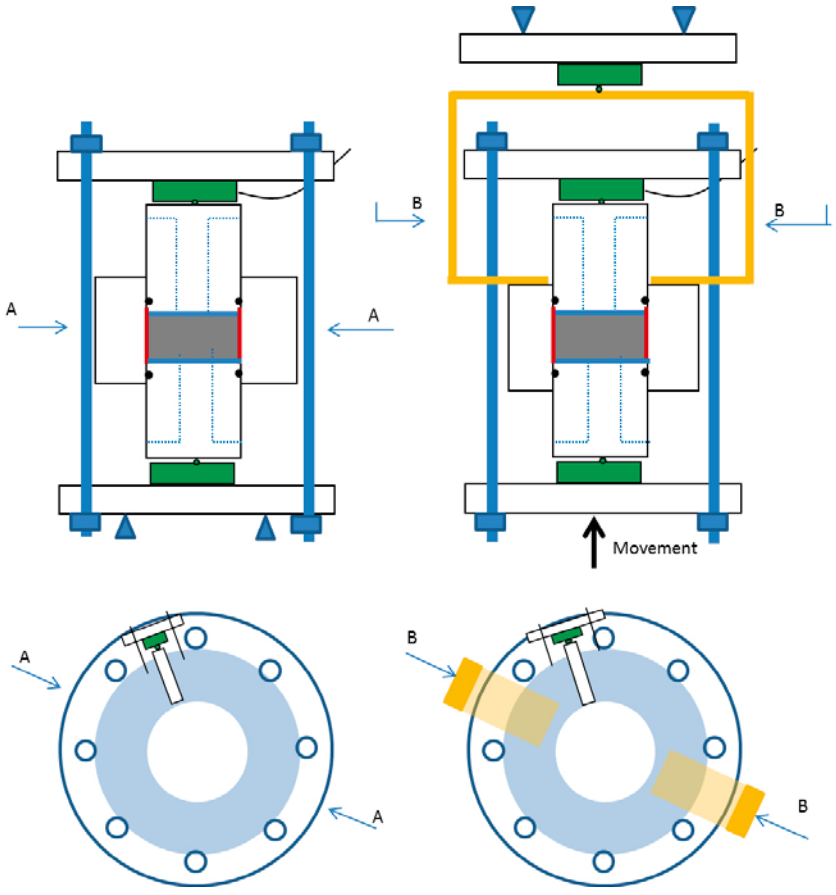

Figure 4-8. *Sketch of the set-up used for the study of friction between the bentonite buffer and other surfaces. The set-up used during saturation (left) and during shearing (right).*

The bottom and top plates are bolted together to keep the volume constant. Three load cells are used for measurements of swelling pressure, two in the vertical direction and one in the radial direction. Each load cell is placed between a fixed plate and a movable piston where the small deformation required by the load cell is admitted. At shearing a third load cell and a deformation transducer are installed for measuring the force and deformation in the axial direction. The transducer and load cells were calibrated prior to, and checked after, each test.

Preparation of specimen

Cylindrical specimens were prepared by compaction of powder to a prescribed density. The specimens had a diameter of 50 mm and a height of 20 mm.

Test procedure

The tests consisted of two phases; the water saturation and the shearing phase. The entire test was done at constant volume conditions. The saturation started by mounting the specimen in the swelling pressure device (Figure 4-8, left) and applying de-ionized water to the filters after air evacuation of the filters and tubes. When only small change in measured swelling pressure was noticed the friction phase started.

During the shearing phase the swelling pressure device was placed in a load frame (Figure 4-8, right) where the ring was fixed while the specimen was moved upwards with a constant rate, i.e. the specimen was pushed upwards through the ring. The set-up used is also shown in Figure 4-9. During this shearing phase the required force to keep the ring in place as well as the deformation and swelling pressure were measured. The specimen had free access to water during both the saturation and the subsequent friction phase. After moving the specimen a distance similar to the height of the specimen the test was finished and the bentonite specimen was dismantled. The of water content and density were then determined.

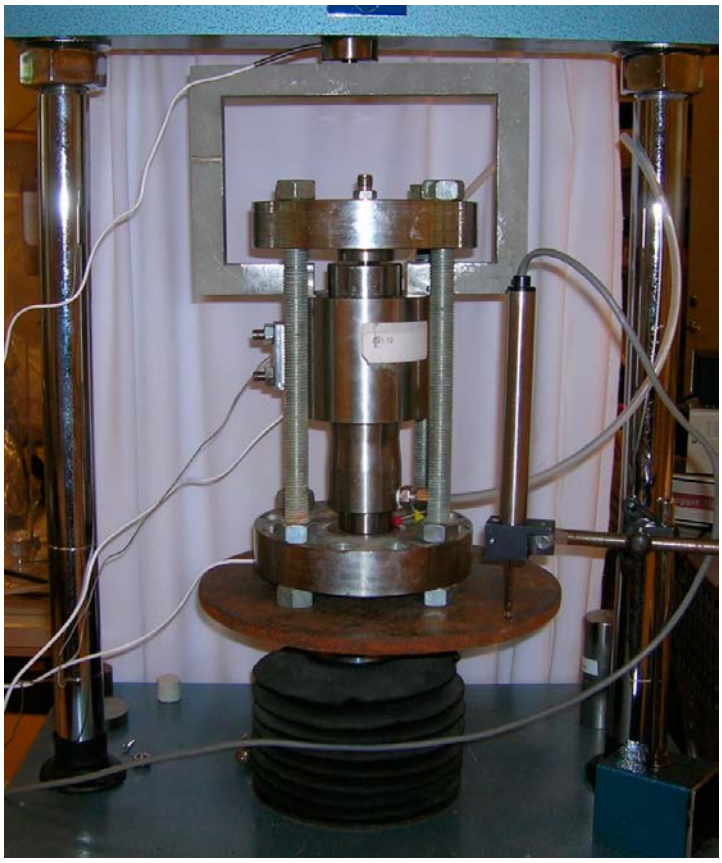

Figure 4-9. *Photo of the set-up during the shearing phase of the test.*

Test results

The friction was evaluated from Equation 4-2 where F is the measured force from the upper load cell, A_s is the radial surface area of the specimen, P_r is the radial stress perpendicular to the ring, and δ is the friction angle between the ring and the bentonite specimen. The swelling pressure and friction angle are presented with average values of w, ρ_d and S_r over the specimens.

$$F = A_s \cdot P_r \cdot \tan(\delta) \qquad \text{(Equation 4-2)}$$

Test series

The specimens were saturated with a minimum of swelling and the friction tests were run with and without lubricant on the inner surface of the ring, surrounding the specimen.

5 Results

5.1 General

The results from all these test series are presented in Sections 5.2 to 5.4. From the two fundamental test series the presentations consist of diagrams with distribution of w, ρ_d and S_r in the direction of swelling. These presentations also contain diagrams of the axial and radial stresses, as a function of ρ_d, measured both after the initial water saturation at constant volume condition and after the subsequent swelling. The stresses are compared with a model derived by Börgesson et al. (1995) (labeled TR-95-20 in the diagrams below). In some diagrams the results are also compared with test results presented by Karnland et al. (2006) (labeled TR-06-30).

Details from the fundamental tests in the basic series are presented in Appendices 1–3 where Appendix 1 contains diagrams of measured stresses as a function of time, Appendix 2 contains tables of the distribution of water content and density over the specimens after dismantling and Appendix 3 contains a sum-up of the final values of average water content, average density, swelling pressure and the total time used for each test.

Details from the fundamental tests in the high resolution series are presented in Appendix 4 where a sum-up of the final values of average water content, average density, swelling pressure and the total time used are given for the two tests run so far.

In Appendix 5 diagrams of the results from the test series with measurement of friction between buffer and other surfaces are given. The evolution of swelling pressure and the evaluated angle of friction as a function of deformation are shown.

The denomination of each specimen (the specimen ID) contains information about the test type, serial number and specimen number, e.g. A01-12 refers to specimen number 12 exposed to axial swelling, A0, in series 1.

5.2 Fundamental swelling tests – basic series

The labels in the diagrams with results include the specimen ID and the swelling in %. The colors blue, green, yellow and red denote swelling 0–10%, 11–20%, 21–30% and 31–40%, respectively, in the diagrams which show water content, dry density and degree of saturation. The amount of swelling was calculated from the initial and final dry densities according to Equation 4-1. In the tables the amount of swelling is also given as swelling after saturation (given in brackets) calculated from the volume before and after the swelling. The difference between the values is mainly caused by a small scatter in the initial density, swelling between the saturation phase and swelling phase and swelling at dismantling.

In the diagrams which show swelling pressure versus dry density the colors blue and red denote the axially and radially measured stresses. In these diagrams the values at high density are the measured values after the first phase, i.e. the saturation.

Axial swelling

The completed tests of axial swelling are shown in Table 5-1. In Figure 5-1 to Figure 5-3 the distribution of w, ρ_d and S_r measured after termination of each test are shown.

The measured axial and radial stresses are shown in Figure 5-4 and Figure 5-5 as a function of dry density. The axial and radial stresses from each test were measured after the first saturation at constant volume condition and after the subsequent swelling. The radially measured stress are presented with the dry density evaluated at the position of the radial piston. The axially measured stress are given with bars showing maximum and minimum dry densities.

Table 5-1. Specimens used in the series A01.

	Initial w (%)	Initial ρ_d (kg/m^3)	Constant Radius (mm)	Height at compaction (mm)	Swelling[1] $\rho_{di}/\rho_{df}-1$ (%)	Remarks
A01-12	13	1,660	25	20	6 (4)	
A01-13	13	1,655	25	20	16 (14)	

[1] Swelling after saturation calculated from volumes, in brackets.

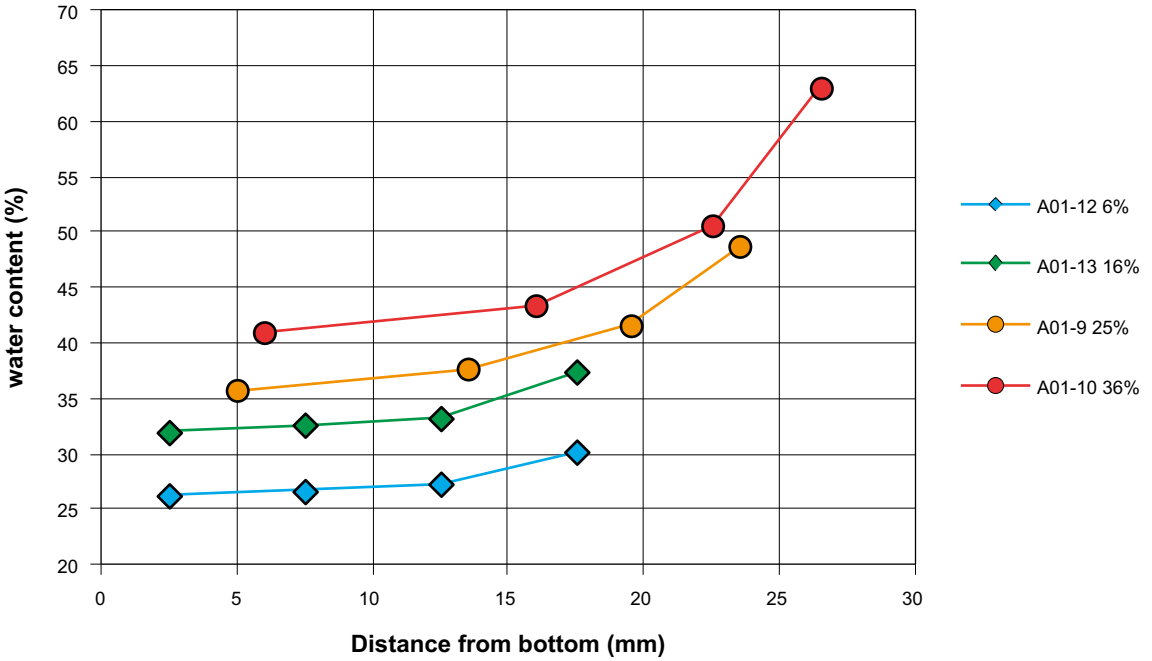

Figure 5-1. Distribution of water content over the specimen height from series A01. The labels denote the type and number of specimen and the last figure denotes the swelling (%). Additional two specimens are also shown A01-9 and A01-10 (Dueck et al. 2011) which started from approximately the same conditions and the initial height 20 mm.

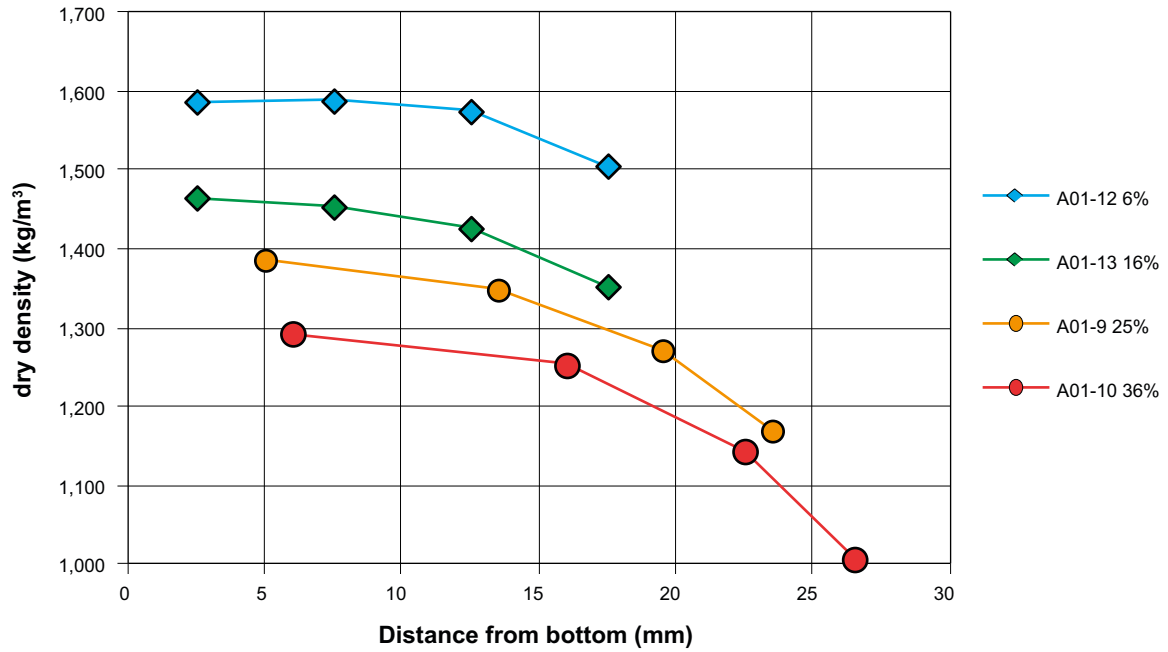

Figure 5-2. Distribution of dry density over the specimen height from series A01. Additional two specimens are also shown A01-9 and A01-10 (Dueck et al. 2011).

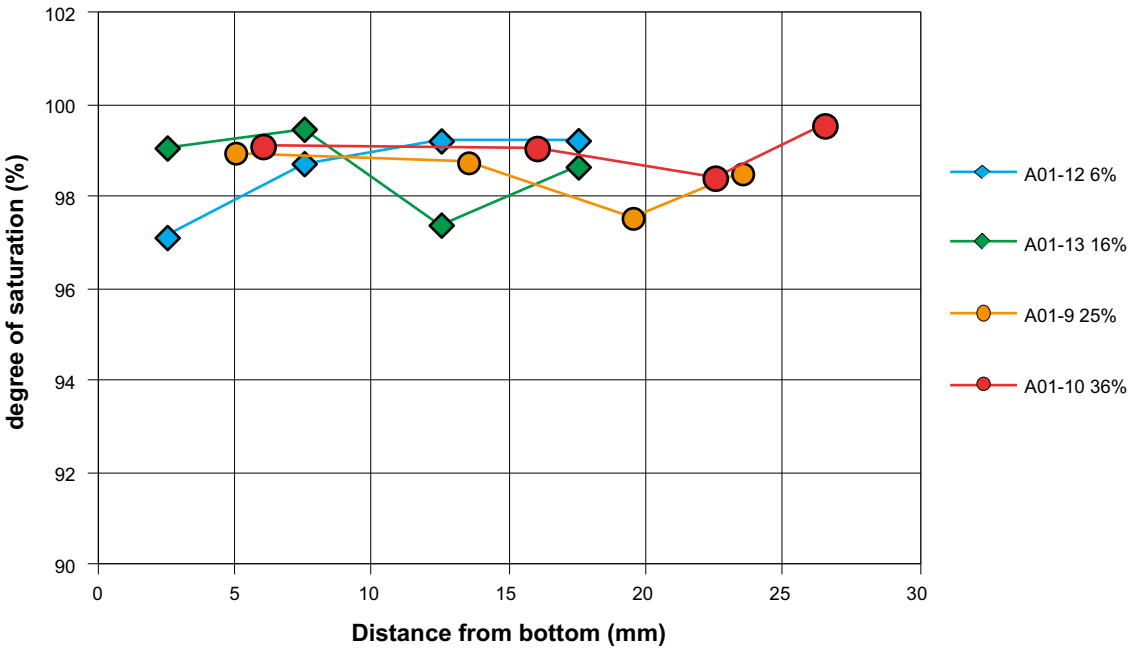

Figure 5-3. *Distribution of degree of saturation over the specimen height from series A01. Additional two specimens are also shown A01-9 and A01-10 (Dueck et al. 2011).*

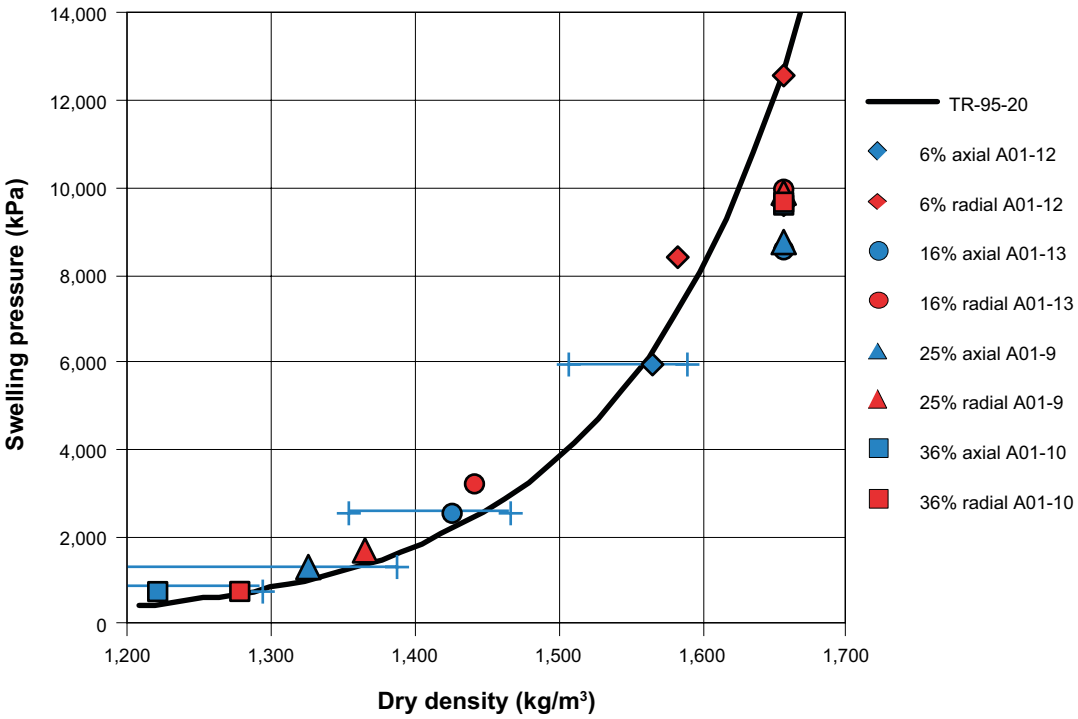

Figure 5-4. *Measured axial and radial stresses in tests A01-12 and A01-13. Results from A01-9 and A01-10 are also shown (Dueck et al. 2011). The labels denote the swelling (%), the direction of measured stress and the specimen ID.*

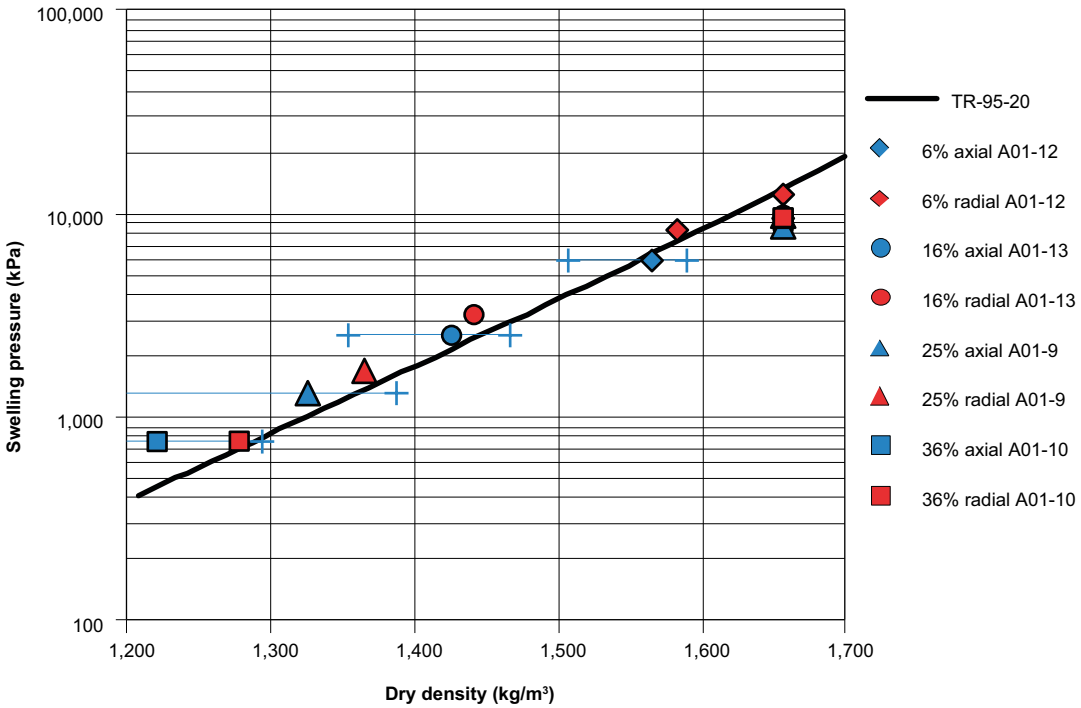

Figure 5-5. *Measured axial and radial stresses from Figure 5-4 are shown with logarithmic y-axis.*

Radial outward swelling

Radial outward swelling of the outer circumferential surface was studied in the tests shown in Table 5-2. In Figure 5-6 to Figure 5-8 the distributions of w, ρ_d and S_r determined after termination are shown. The values are plotted as a function of the radius but since the determination was made on a strip, and not on a circular specimen, each value represents an average over a strip with a thickness of approximately 8 mm and an extension in the perpendicular radial direction corresponding to approximately half the diameter, i.e. 25 mm, cf Figure 5-22.

In addition to the compacted specimens used in this test series one specimen was sampled radially from a larger compacted block; R11-21. The dry density of the specimens after compaction was between 1,720 kg/m^3 and 1,740 kg/m^3. The initial dry densities given in Table 5-2, however, represent the initial state of the swelling phase when the specimen fills the volume and the small initial gaps, needed for the mounting, are no longer present. Regarding R11-21 the density after the first saturation phase was uncertain.

The stresses measured after the saturation phase and after the swelling in each test are shown in Figure 5-9 and Figure 5-10 as axial and radial stresses as a function of the average dry density. From each test two pairs of axial and radial stresses are shown which represent the stresses under constant volume condition and the stresses after subsequent swelling. The bars denote the maximum and minimum densities measured after dismantling.

Table 5-2. Specimens used in the series R11.

	Initial w (%)	Initial ρ_d (kg/m^3)	Constant height (mm)	Initial diameter (mm)	Final diameter (mm)	Swelling[1] $\rho_{di}/\rho_{df}-1$ (%)	Remarks
R11-17	13	1,716[2]	40	43.8	46.8	17	swelling directly, no initial saturation
R11-18	13	1,655	40	43.8	46.8	18 (14)	
R11-19	13	1,655	40	40.8	46.8	32 (32)	
R11-20	13	1,655	40	40.8	46.8	32 (32)	Compacted in two instead of one piece
R11-21	13	1,721	40	40.8	46.8	31 (32)	Radially sampled from larger block

[1] Swelling after saturation calculated from volumes, in brackets. [2] Approximate density.

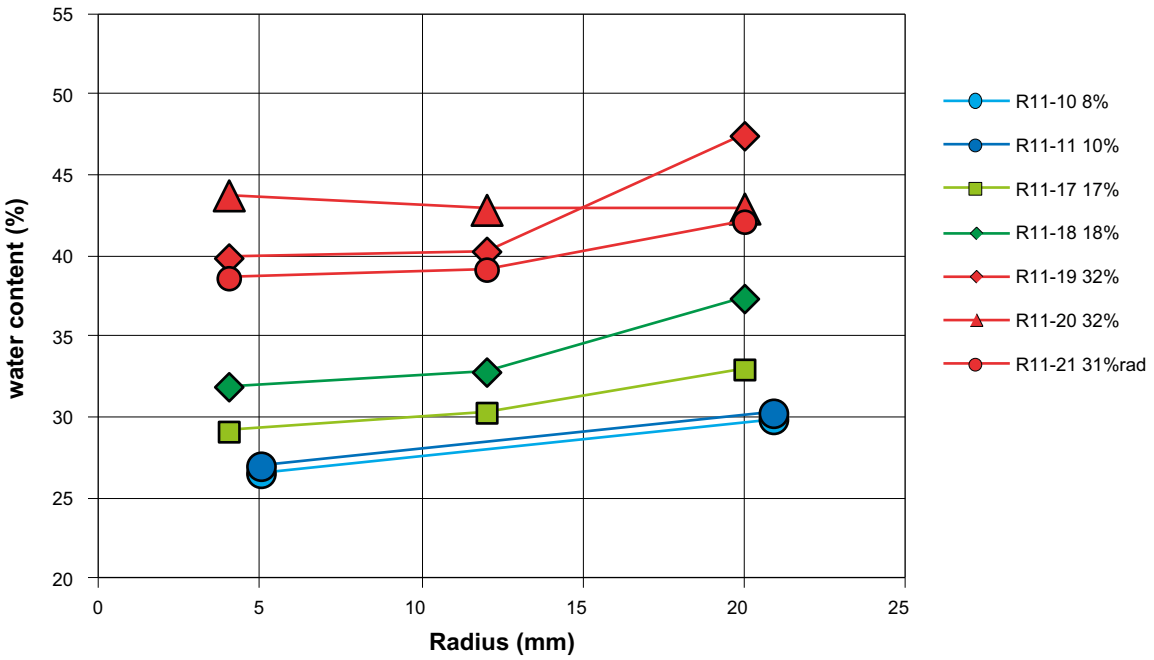

Figure 5-6. *Distribution of water content over the radius of the specimens from series R11. The labels denote the type and number of specimen and the last figure denotes the swelling (%). Results from R11-10 and R11-11 (Dueck et al. 2011), swelling from approximately the same density as R11-17 to the same final volume, are also shown.*

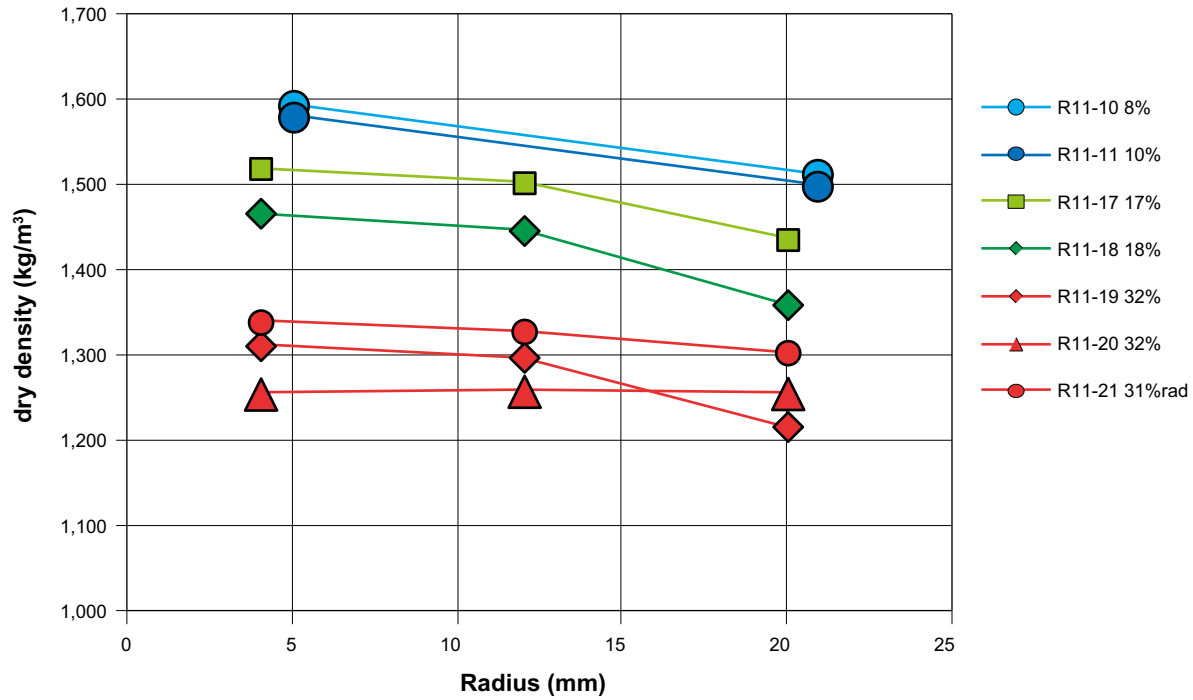

Figure 5-7. *Distribution of dry density over the radius of the specimens from series R11. Results from R11-10 and R11-11 (Dueck et al. 2011) are also shown.*

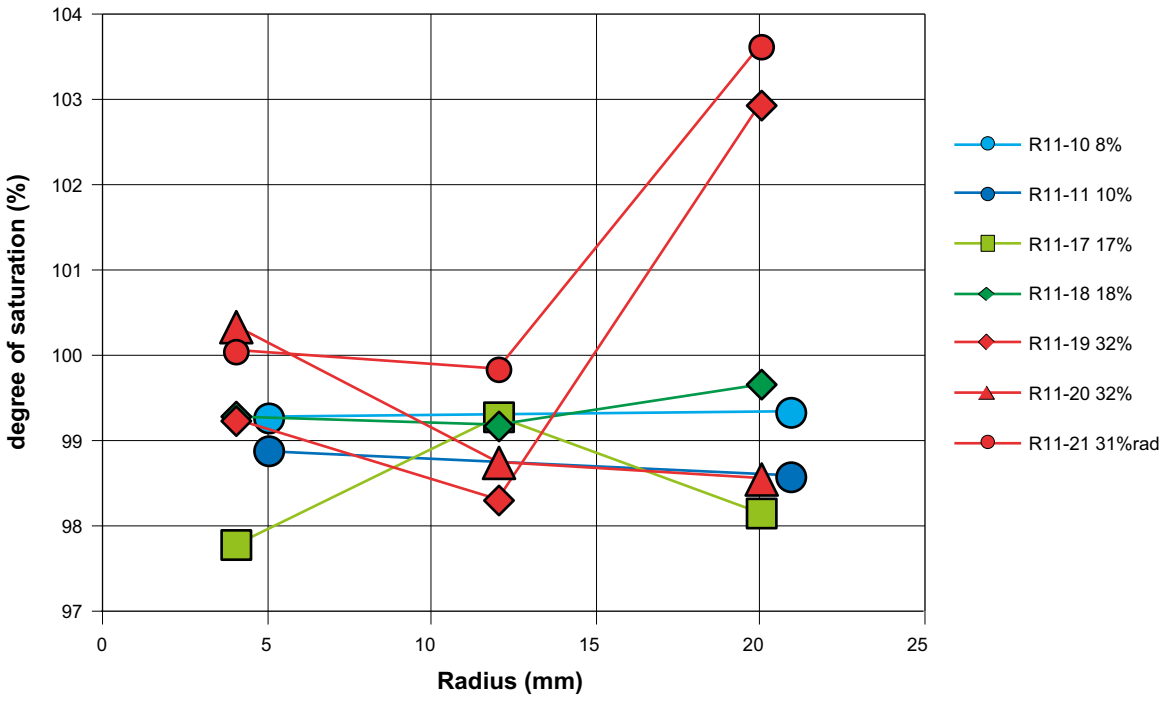

Figure 5-8. *Distribution of degree of saturation over the radius of the specimens from series R11. Results from R11-10 and R11-11 (Dueck et al. 2011) are also shown.*

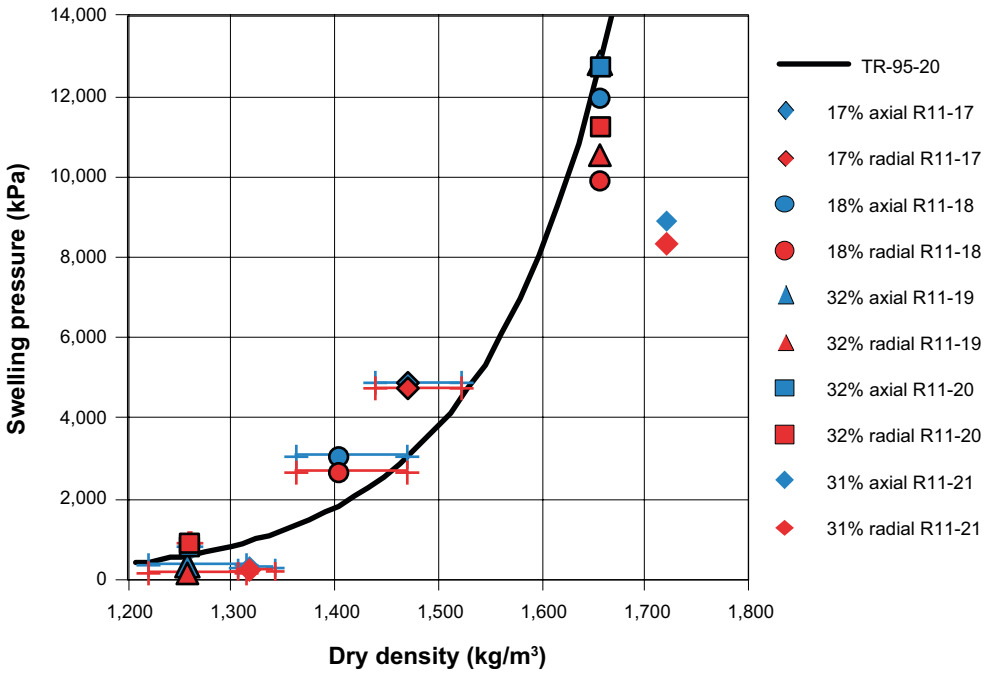

Figure 5-9. *Measured axial and radial stresses from tests R11-17 to R11-21. The labels denote the swelling (%), the direction of measured stress and the specimen ID. Regarding R11-21 the density after the first saturation phase was uncertain.*

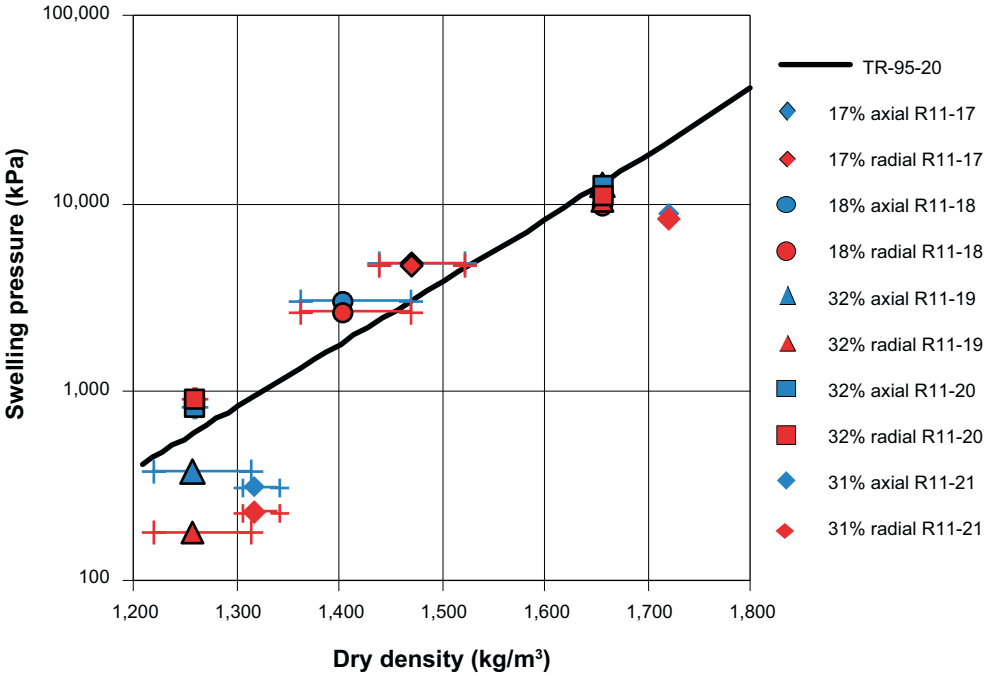

Figure 5-10. *Measured axial and radial stresses from tests R11-17 to R11-21 with logarithmic y-axis.*

Radial inward swelling

Radial swelling into a cavity was studied in the tests shown in Table 5-3. The distributions of w, ρ_d and S_r determined after termination are shown in Figure 5-11 to Figure 5-13. The values are plotted as a function of the radius but since the determination was made on a strip, and not on a circular specimen, each value represents an average over a strip according to the description in section Radial outward swelling, see also Figure 5-22.

The dry density after compaction was approximately 1,720 kg/m^3 and the initial dry densities given in Table 5-3 represent the initial state of the swelling phase when the specimen fills the volume and the small initial gaps, needed for the mounting, are no longer present.

The measured stresses during each test are shown in Figure 5-14 and Figure 5-15 as axial and radial stresses as a function of dry density. The axial and radial stresses from each test were measured after completed water saturation at constant volume condition and after the subsequent swelling. The bars denote the maximum and minimum densities measured after dismantling.

Table 5-3. Specimens used in the series R21.

	Initial w (%)	Initial ρ_d (kg/m^3)	Constant height (mm)	Outer radius (mm)	Cavity diameter (mm)	Swelling[1] $\rho_{di}/\rho_{df}-1$ (%)	Remarks
R21-9	13	1,655	40	46.8	10.5	6 (5)	
R21-10	13	1,656	40	46.8	19	23 (20)	
R21-11	13	1,657	40	46.8	8	4 (3)	
R21-12	13	1,660	40	46.8	23	31 (32)	

[1] Swelling after saturation calculated from volumes, in brackets.

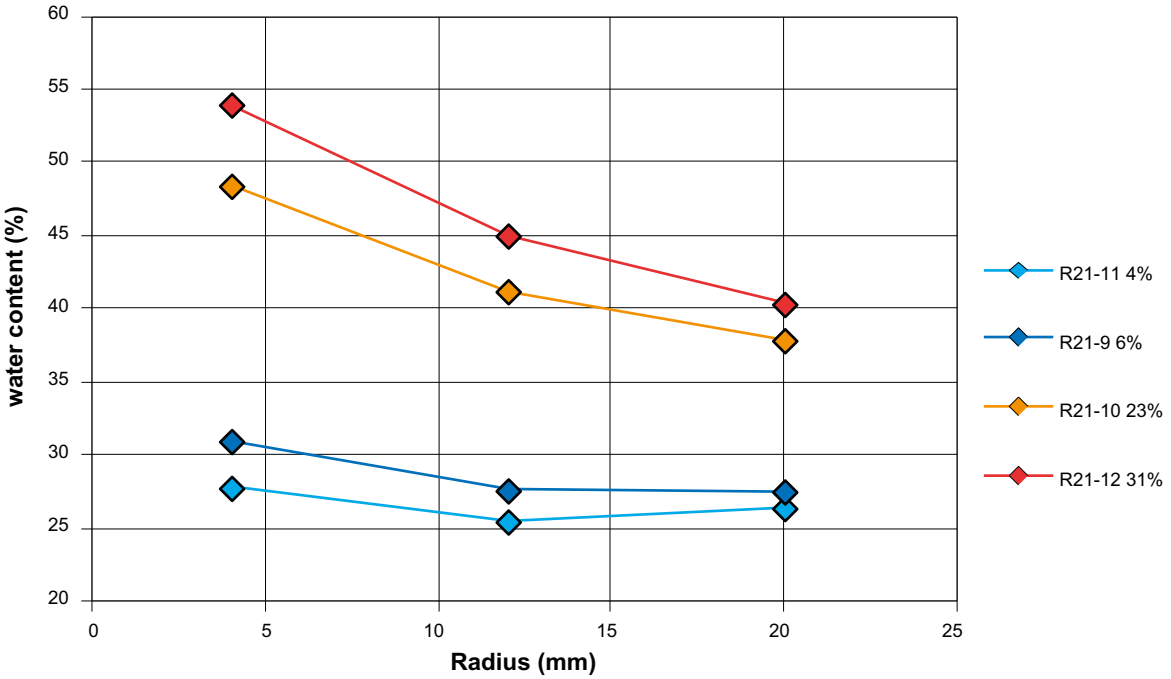

Figure 5-11. *Distribution of water content over the radius of the specimens from series R21. The labels denote the type and number of the specimen and the last figure denotes the swelling (%).*

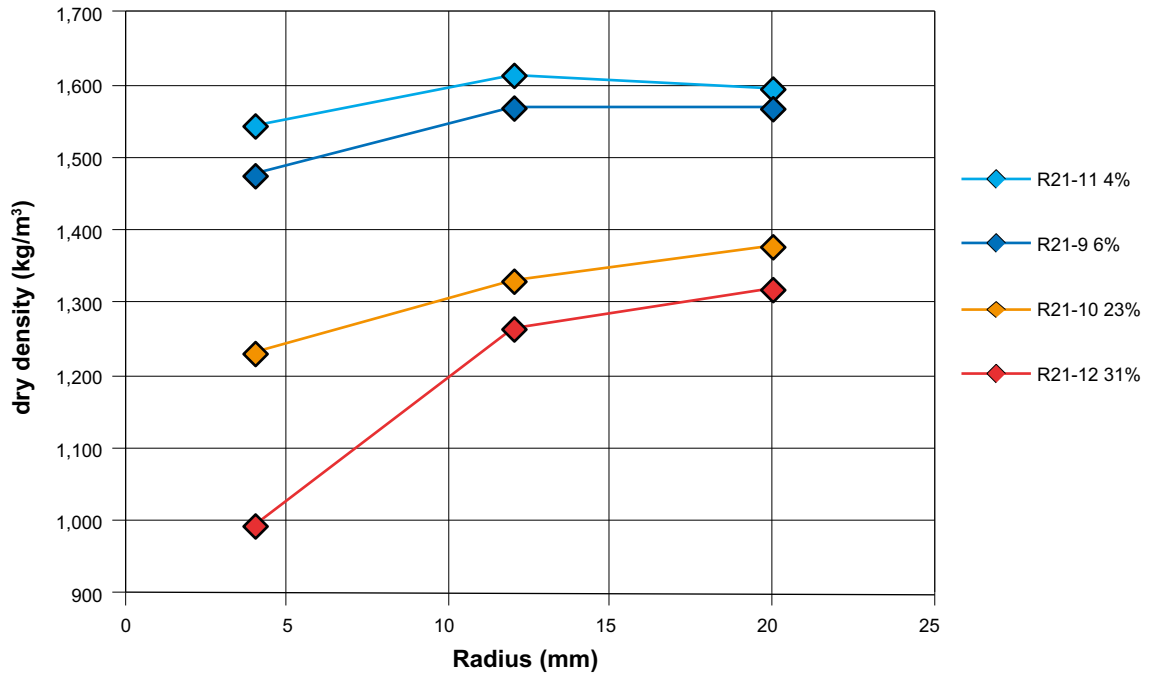

Figure 5-12. *Distribution of dry density over the radius of the specimens from series R21.*

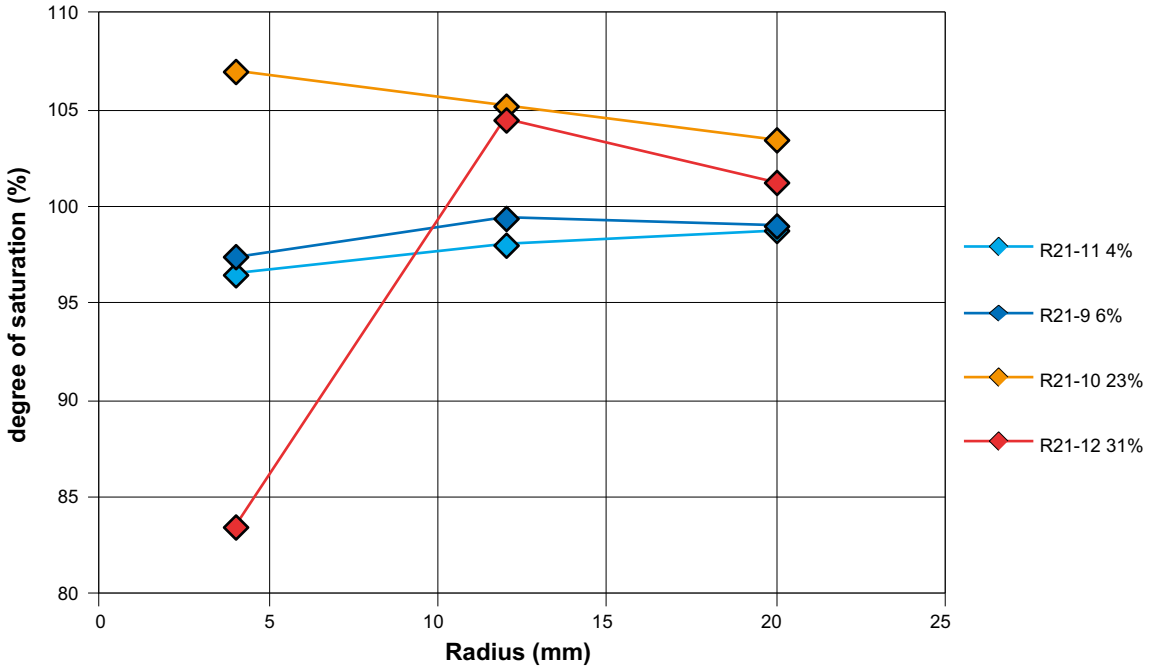

Figure 5-13. *Distribution of degree of saturation over the radius of the specimens from series R21.*

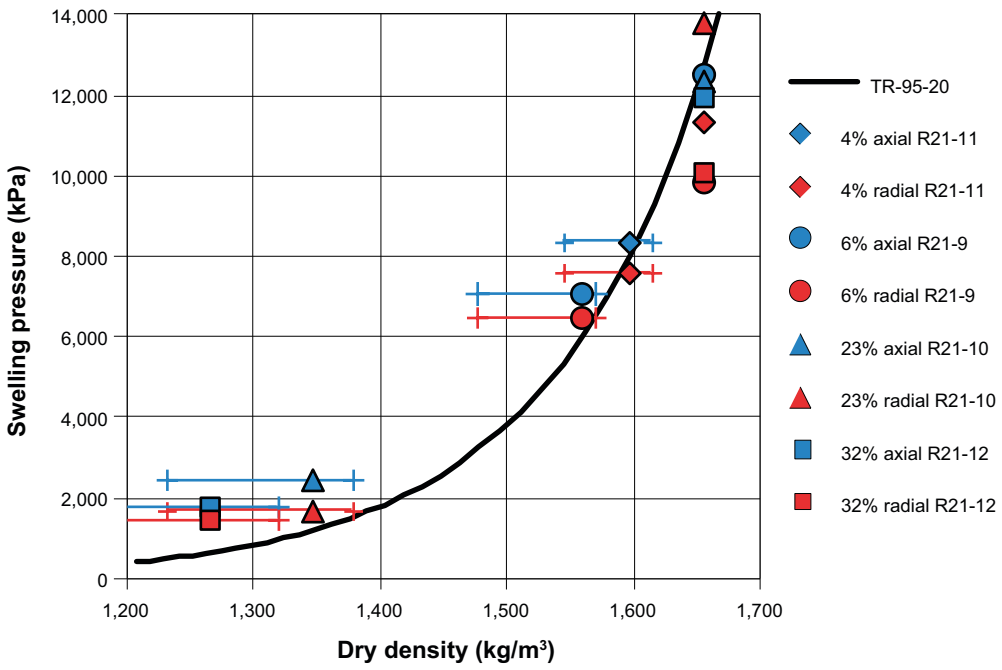

Figure 5-14. *Measured axial and radial stresses from tests from series R21. The labels show swelling (%), the direction of the measured stress and the specimen ID.*

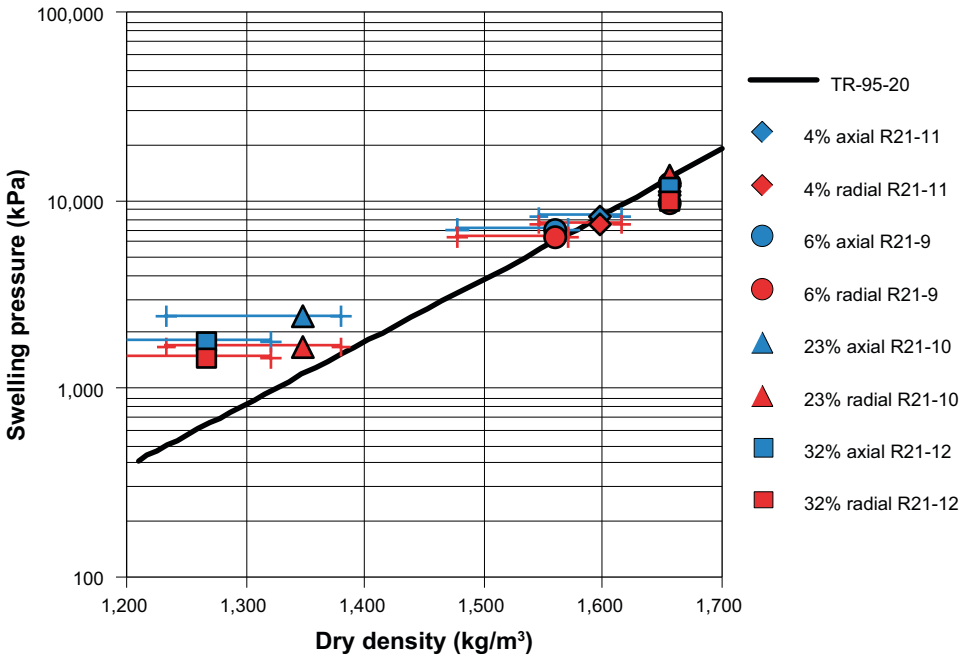

Figure 5-15. *Measured axial and radial stresses from all tests from series R21 with logarithmic y-axis.*

Observations

In general the main purpose of the report was to provide results that can be used for modelling, but the following observations could also be made:

- The gradients in w and ρ_d clearly increased with the total amount of swelling (4%–32%) in case of axial swelling and radial inward swelling, see Figure 5-16. For the radial outward swelling the largest swelling of 32% deviated from this in that the same or lower gradient as resulting from 10% of swelling was observed.
- A high degree of saturation was achieved in all specimens; the average degree of saturation was larger than 98% which indicate full saturation. Extreme values, 84% or 107%, were seen on samples from the most swelling parts where the accuracy may be less good.
- The stresses corresponded fairly well with the swelling pressure from the model presented by Börgesson et al. (1995). The best correspondence was seen from the axial swelling. From the radial swelling the best correspondence with the model was seen when the measured stresses were combined with the largest represented density except from two specimen exposed to radial outward swelling (R11-19 and R11-21).
- The swelling pressure after swelling measured in the direction perpendicular to the swelling was of the same size or larger than was measured in the direction of swelling.

5.3 Fundamental swelling tests – high resolution

The labels in the diagrams with results include the swelling in %. The swelling was calculated from the initial and final dry densities according to Equation 4-1. The swelling was also given as swelling after saturation (given in brackets in the tables) calculated from the volume before and after swelling. The difference between the values is mainly caused by a small scatter in the initial density, swelling between the saturation phase and swelling phase and swelling at dismantling. Also given in the labels used in the diagrams and in addition to the swelling in % is the specimen ID or the position of the actual measurement.

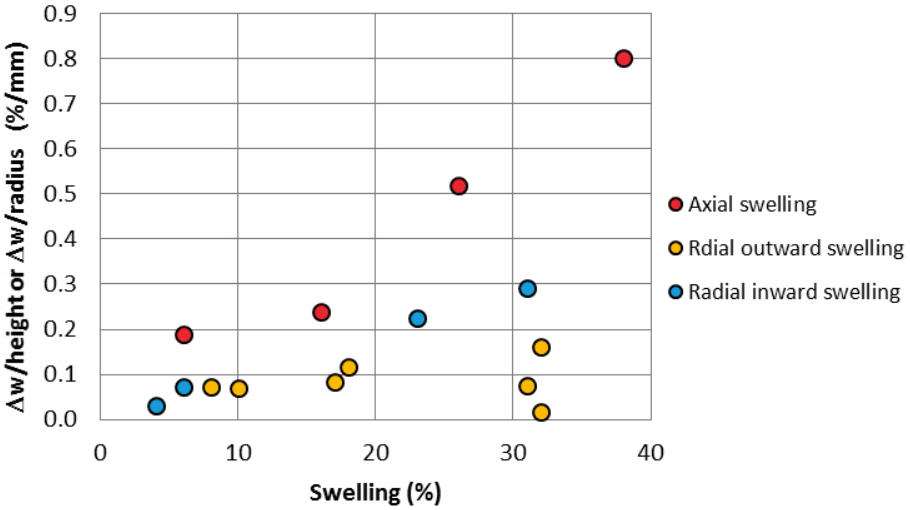

Figure 5-16. *Difference in water content over sample height or radius as a function of the amount of swelling.*

Axial swelling

In the series with axial swelling in the high resolution series one test has been completed, Table 5-4. In Figure 5-17 to Figure 5-19 the distribution of w, ρ_d and S_r measured after termination of the test are shown. The results are shown with comparable test results from the basic series.

Table 5-4. Specimens used in the series HR-A.

	Initial w (%)	Initial ρ_d (kg/m^3)	Constant diameter (mm)	Initial height (mm)	Final height (mm)	Swelling[1] $\rho_{di}/\rho_{df}-1$ (%)	Remarks
HR-A1	23.7	1,666	100	40	50	32 (26)	

[1] Swelling after saturation calculated from volumes, in brackets.

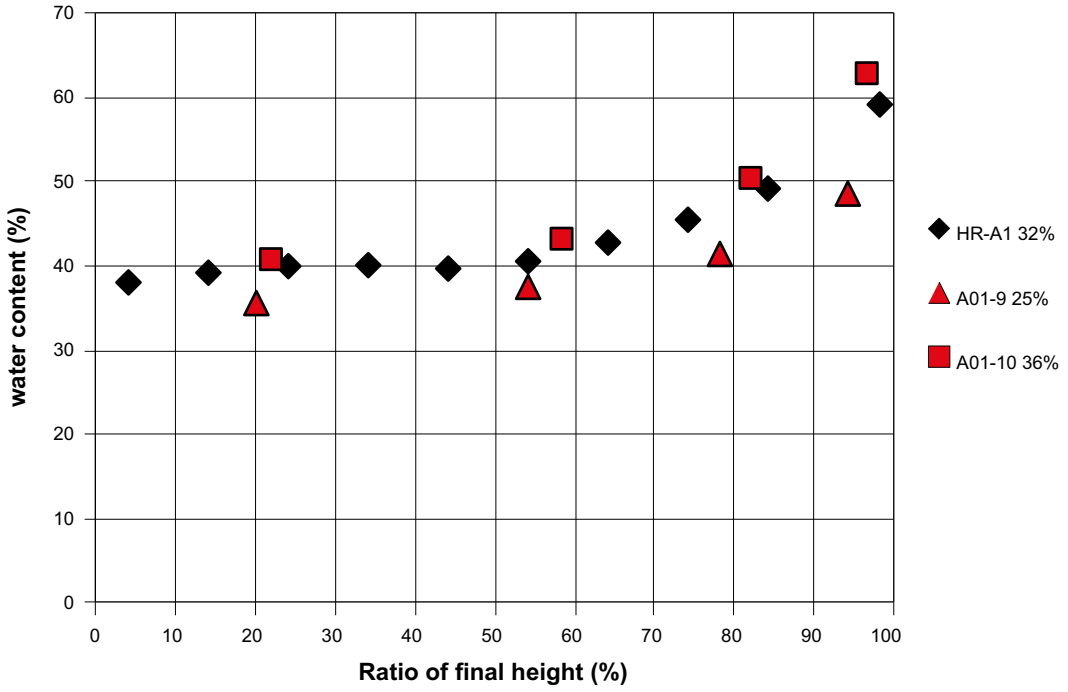

Figure 5-17. *Distribution of water content over specimen height, from bottom end surface. Result from HR-A1 is shown with results from the basic series; A01-9 and A01-10 (cf Figure 5-1).*

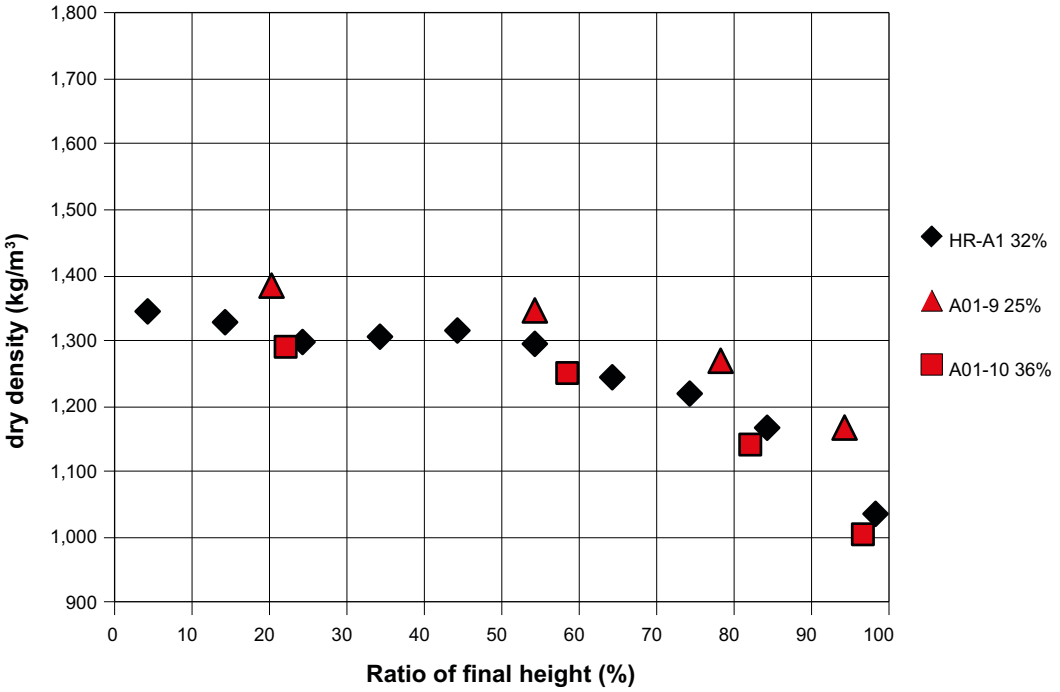

Figure 5-18. *Distribution of dry density over specimen height, from bottom end surface. Result from HR-A1 is shown with results from the basic series; A01-9 and A01-10 (cf Figure 5-2).*

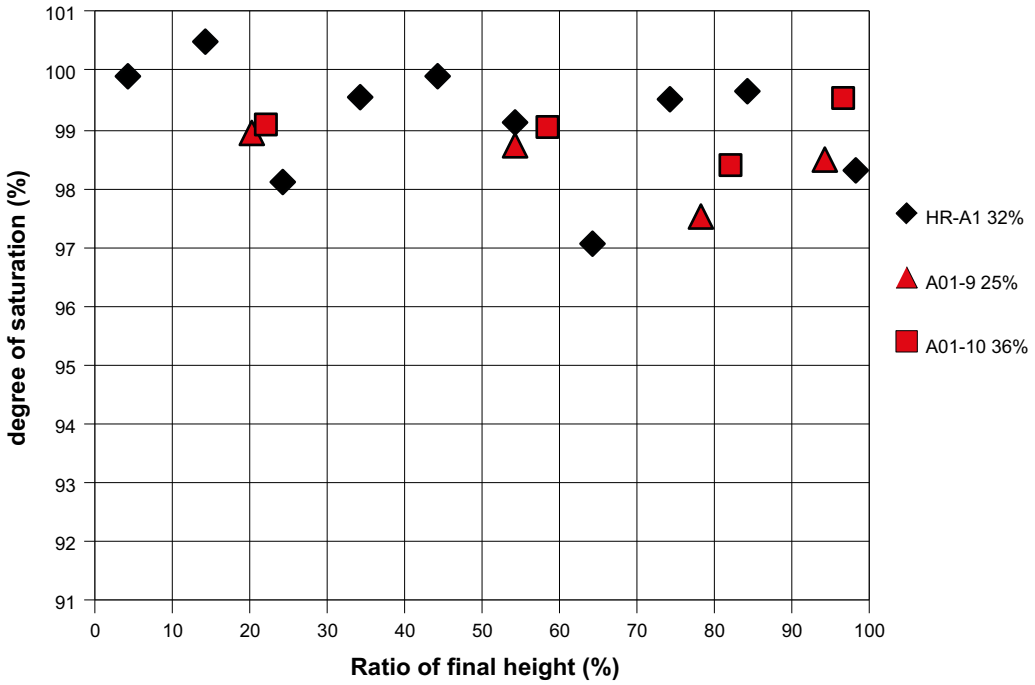

Figure 5-19. *Distribution of degree of saturation over specimen height, from bottom end surface. Result from HR-A1 is shown with results from the basic series; A01-9 and A01-10 (cf Figure 5-3).*

The time evolution of the swelling pressure is shown in Figure 5-20. In Figure 5-21 the swelling pressure is plotted as a function of dry density. The radially measured stress from test HR-A1 are plotted with the dry densities measured at the corresponding distances from the bottom surface. The axially measured stress from test HR-A1 is plotted with the average dry density and a bar corresponding to the maximum and minimum dry densities over the specimen height. In addition, results from the basic test series are shown.

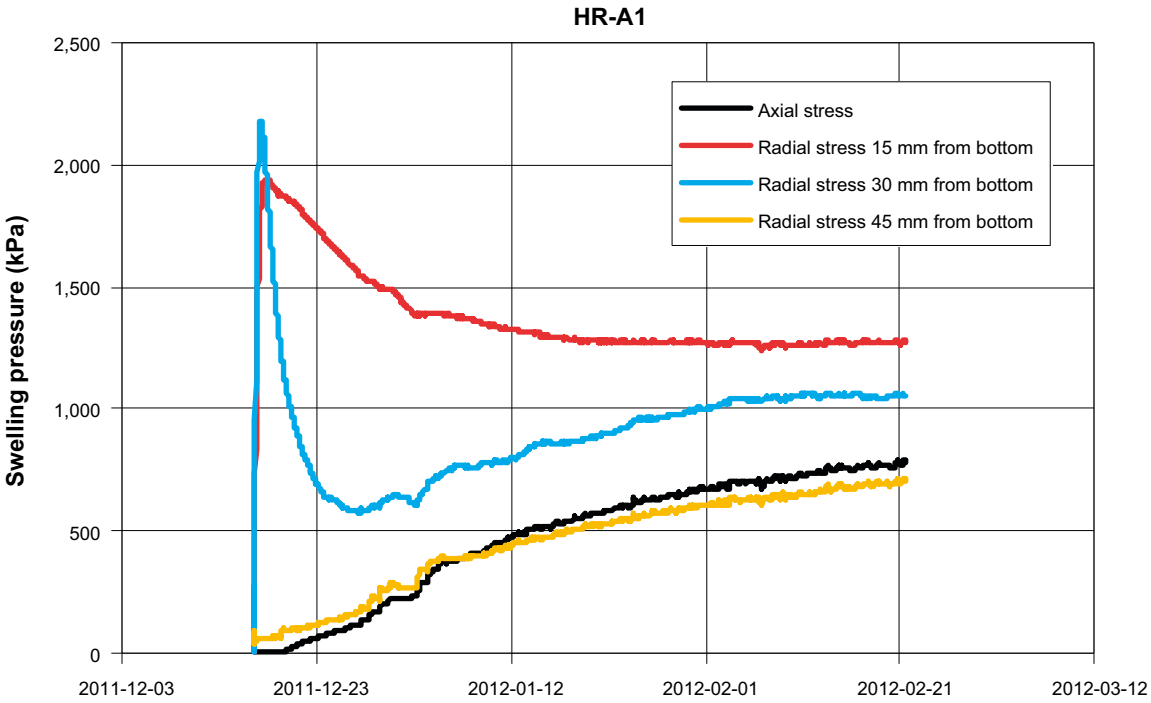

Figure 5-20. *Time evolution of the swelling pressure from test HR-A1.*

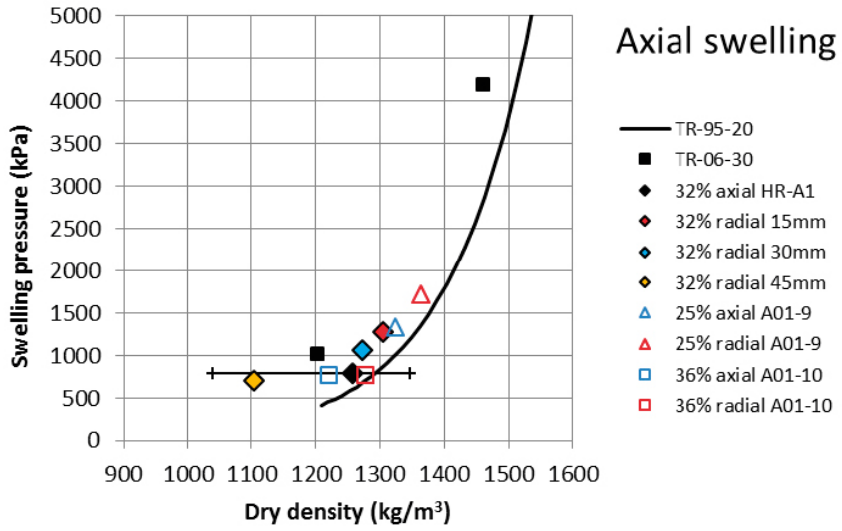

Figure 5-21. *Swelling pressure plotted as a function of dry density. The radially measured stresses are plotted with the dry density measured at the corresponding locations. Axially measured stresses are plotted with the average dry density. Also shown are results from the basic series; A01-09 and A01-10 (cf Figure 5-4).*

Radial outward swelling

In the series with radial swelling in the high resolution series one test has been completed, Table 5-5. In Figure 5-23 to Figure 5-25 the distribution of w, ρ_d and S_r measured after termination of the test are shown. The values are plotted as a function of the radius but since the determination was made on a strip, and not on a circular specimen, each value represents an average over a strip according to Figure 5-22 and does not correspond to the exact radius.

Table 5-5. Specimens used in the series HR-Ro.

	Initial w (%)	Initial ρ_d (kg/m^3)	Constant height (mm)	Initial diameter (mm)	Final diameter (mm)	Swelling[1] $\rho_{di}/\rho_{df}-1$ (%)	Remarks
HR-Ro1	23.7	1,666	80	81	96.8	42 (43)	

[1] Swelling after saturation calculated from volumes, in brackets.

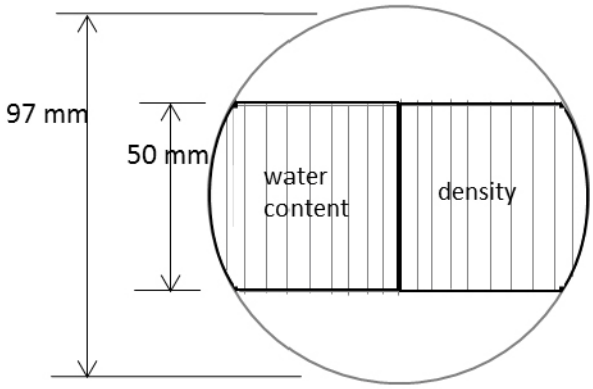

Figure 5-22. *Outline of the sampling of specimens swelling radially, HR-Ro1.*

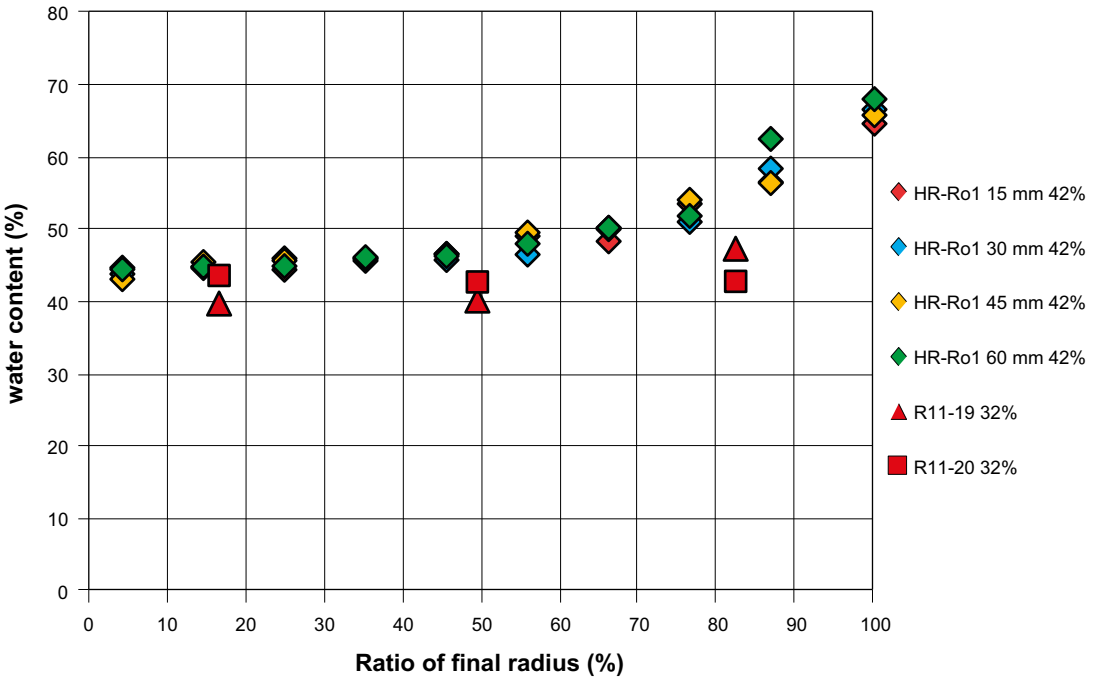

Figure 5-23. *Distribution of water content over the radius. Result from HR-Ro1 is shown with results from the basic series; R11-19 and R11-20 (cf Figure 5-6).*

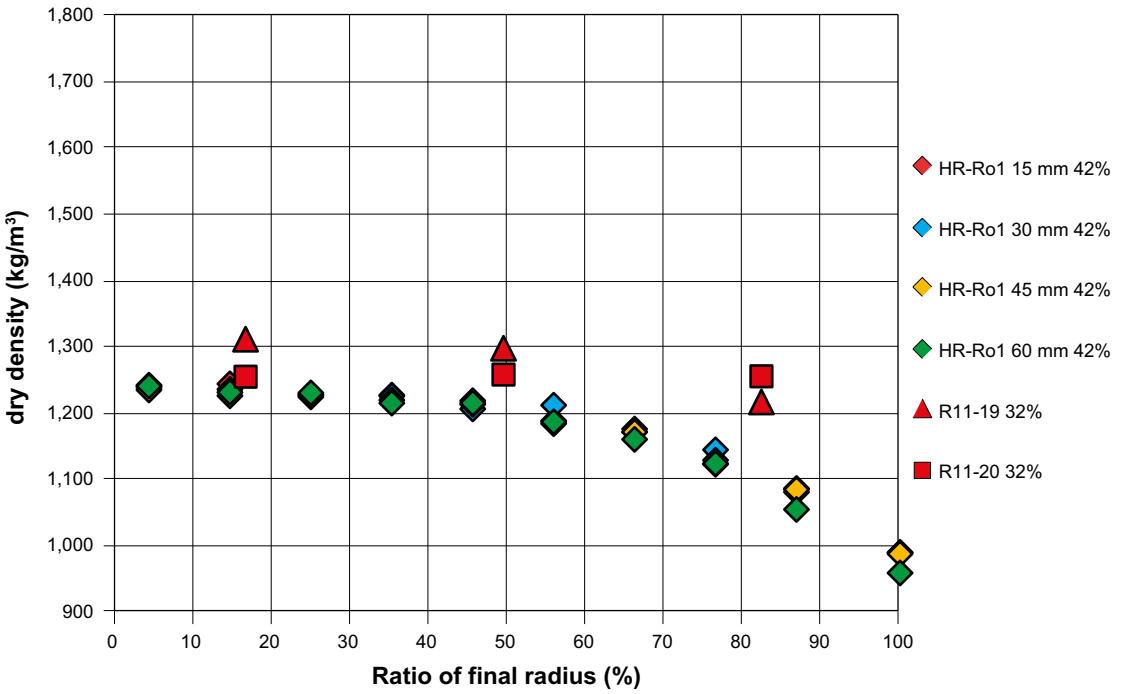

Figure 5-24. *Distribution of dry density over the radius. Result from HR-Ro1 is shown with results from the basic series; R11-19 and R11-20 (cf Figure 5-7).*

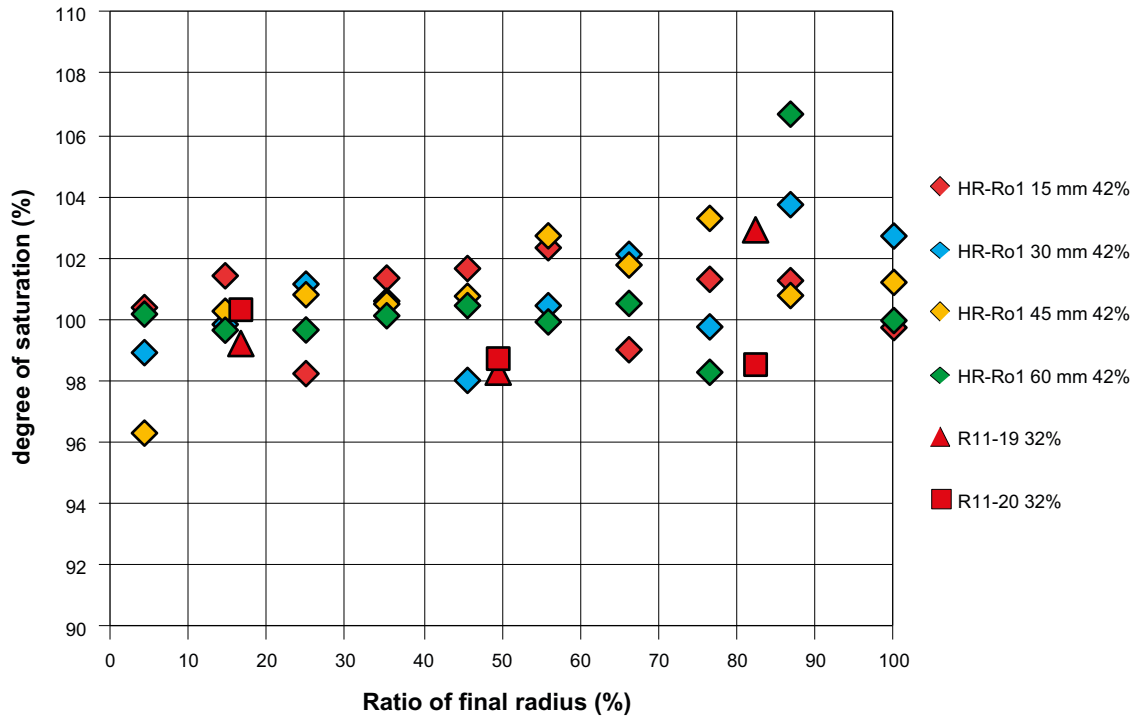

Figure 5-25. *Distribution of degree of saturation over the radius. Result from HR-Ro1 is shown with results from the basic series; R11-19 and R11-20 (cf Figure 5-8).*

The labels shown in the diagrams include the specimen ID and the swelling in %. The results are shown with comparable tests from the basic series.

The time evolution of the swelling pressure is shown in Figure 5-26. In Figure 5-27 the swelling pressure is plotted as a function of dry density. The radially measured stress from test HR-Ro1 are plotted with the dry densities measured at the corresponding distances from the bottom surface. The axially measured stress from test HR-Ro1 is plotted with the average dry density and a bar corresponding to the maximum and minimum dry densities over the radius of the specimen. In addition, results from the basic test series are shown.

Observations

In general the main purpose of the report was to provide results that can be used for modelling, but the following observations could also be made:

- Good agreement was seen in the distribution of w and ρ_d from the larger specimens (HR series) and the smaller specimens (basic series). This indicated small influence of the scale.
- After radial outward swelling the gradients of water content and density seem to be underestimated when evaluated from the smaller specimens (basic series).
- A high degree of saturation was achieved; larger than 98%.
- The stresses corresponded fairly well with the swelling pressure from the model presented by Börgesson et al. (1995), especially when the density present at the location of the transducer was used. The density present at the lowest measured swelling pressure was outside the limit of the model but agreed better with test results presented by Karnland et al. (2006).
- The axially measured stress after 32% of axial swelling was of the same size as the lowest radially measured stress. The axially measured stress after 42% of radial swelling was of the same size as the radially measured stress.

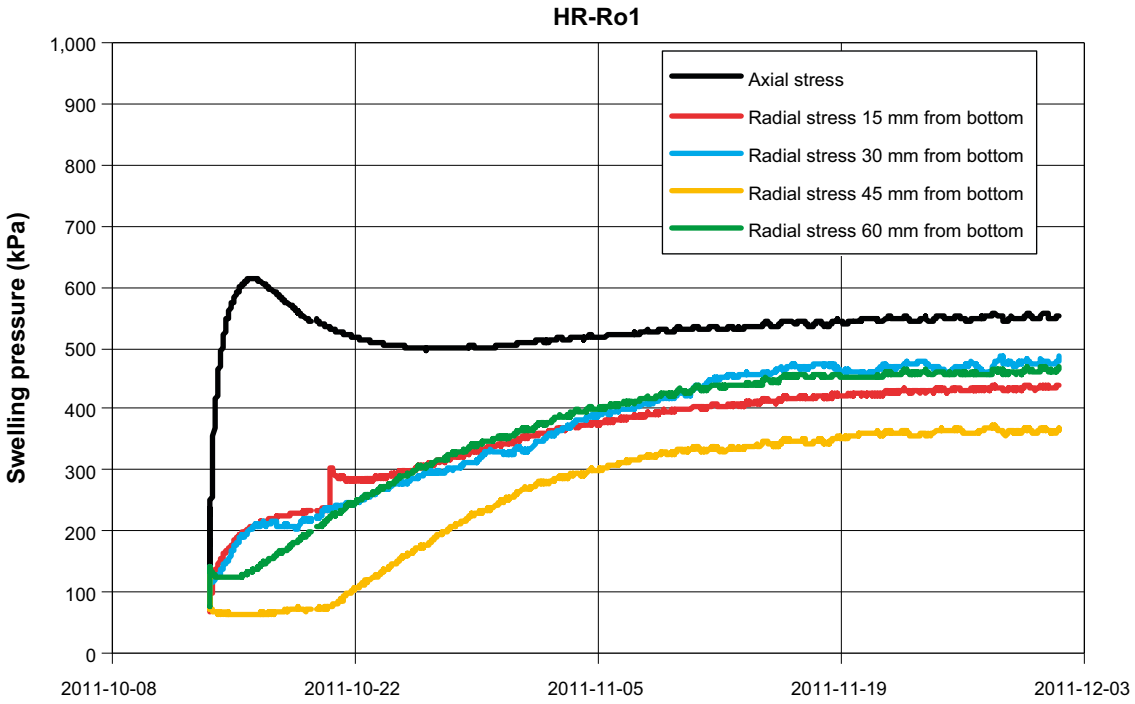

Figure 5-26. *Time evolution of the swelling pressure from test HR-Ro1.*

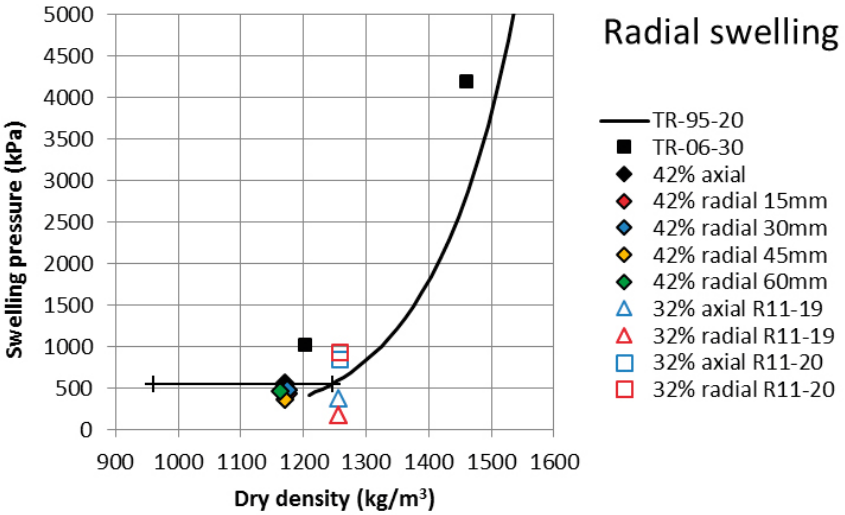

Figure 5-27. *Swelling pressure as a function of dry density. The radially measured stresses are plotted with the average dry density at the corresponding level. Axially measured stresses are plotted with the average dry density over the specimen. Also shown are results from the basic series R11-19 and R11-20 (cf Figure 5-9).*

5.4 Measurements of friction between buffer and other surfaces

Results from the test series where friction between buffer and other surfaces was studied are presented in Table 5-6. The friction angle δ (Equation 4-2) is interpreted both as the peak value at the beginning of the deformation and as the more or less residual value reached after some distance of deformation at a rate of 0.01 mm/min. The swelling pressure used for the evaluation was the radially measured stress, which not always corresponded fully with the axially measured stress, see for example Fr1_1 in Appendix 5. However, in tests Fr1_3 and Fr1_7 no radial stress was measured and for these tests the axially measured stress was used. Test Fr1_6 was considered irrelevant due to rapidly increasing friction force presumably due to an inclined set-up.

The angle of friction δ in Table 5-6 was evaluated at a deformation rate of 0.01 mm/min. In tests Fr1_8 and Fr1_9 other deformation rates were also used and the results are shown in Figure 5-28 and Figure 5-29. No large influence of the deformation rates used; 0.01, 0.1 and 1 mm/min, was seen.

In Figure 5-30 the evaluated angle of friction from Table 5-6 is plotted as a function of swelling pressure. For comparison a relation for the bentonite friction angle ϕ, based on triaxial tests, presented by Åkesson et al. (2010) is given in the diagram. The friction angles of the bentonite/steel interface, evaluated from Equation 4-2, were thus less than the bentonite friction angel.

Table 5-6. Results from measurement of friction between buffer and steel. Evaluated angle of friction δ for the deformation rate 0.01 mm/min and the swelling pressure measured as radial stress. Peak values δ_{peak} are also evaluated. Water content w, dry density ρ_d and degree of saturation S_r after dismantling are given.

Test ID	Friction angle δ (δ_{peak}) °	Swelling pressure kPa	Surface	After dismantling w %	ρ_d kg/m³	S_r %	Remarks
Fr1_1	2.5 (3.6)	14,200	lubricated	24.8	1,630	97	
Fr1_2	4.4 (4.7)	11,070		24.6	1,630	97	
Fr1_3	5.5 (5.9)	12,700	lubricated	24.3	1,640	97	P_a used, δ not levelled out
Fr1_4	5.6 (5.6)	6,280		27.2	1,560	97	
Fr1_5	4.8 (7.8)	2,340		34.6	1,410	99	
Fr1_7	4.1 (5.4)	9,820	lubricated	25.4	1,610	97	P_a used
Fr1_8	6.7 (8.4)	800		47.9	1,190	100	
Fr1_9	5.7 (7.4)	920	lubricated	44.5	1,230	99	δ not levelled out

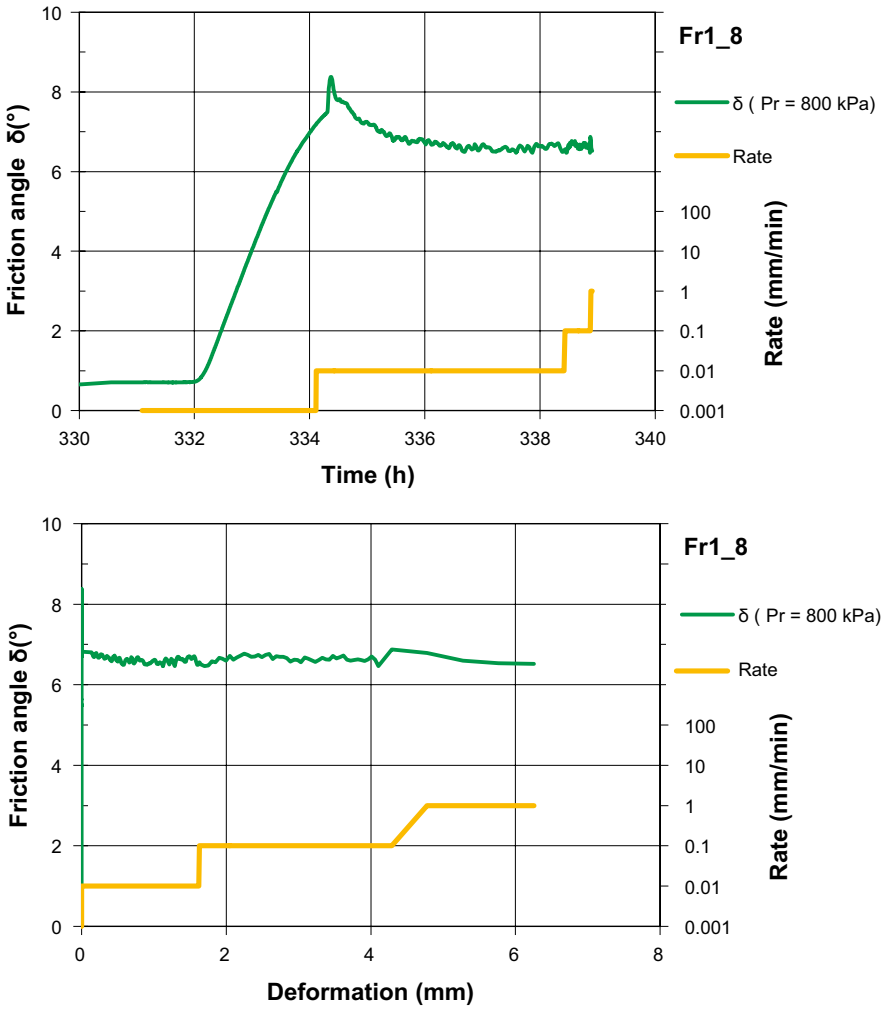

Figure 5-28. *Friction angle at different deformation rates as a function of a. Time and b. Deformation. Results from Fr1_8 where the radially measured stress was 800 kPa and the buffer was in contact with a steel surface.*

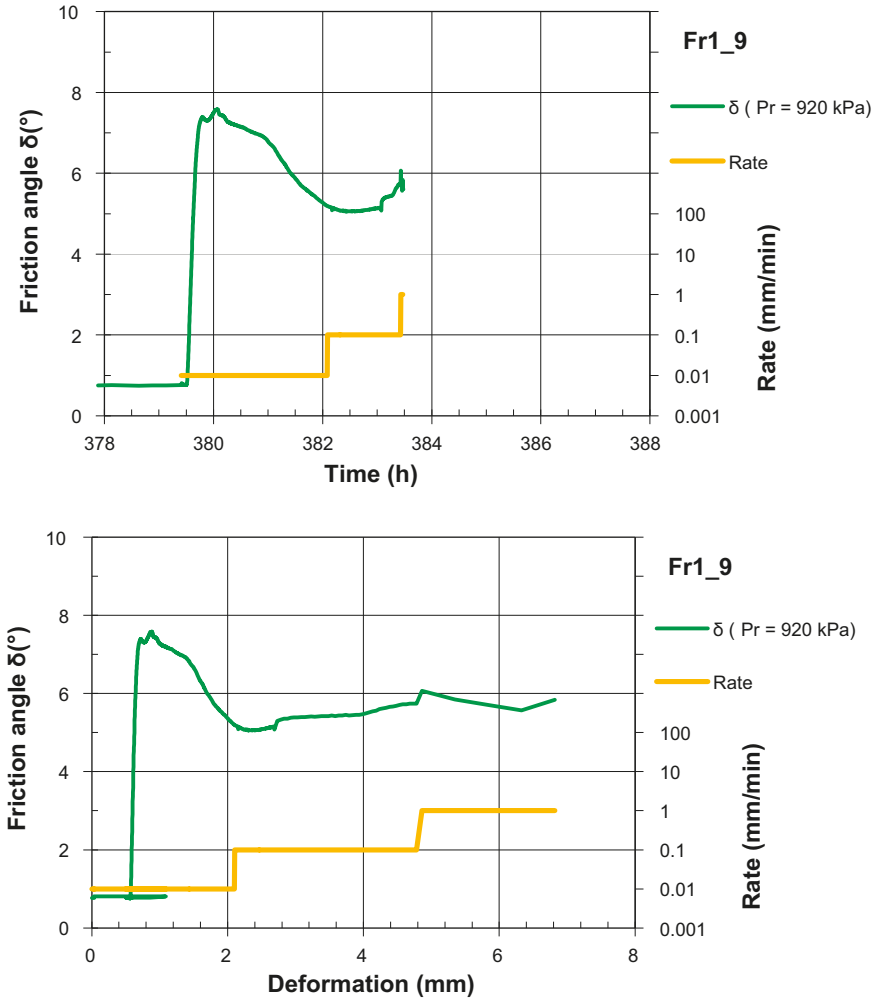

Figure 5-29. *Friction angle at different deformation rates as a function of a. Time and b. Deformation. Results from Fr1_9 where the radial measured stress was 920 kPa and the buffer was in contact with a lubricated steel surface.*

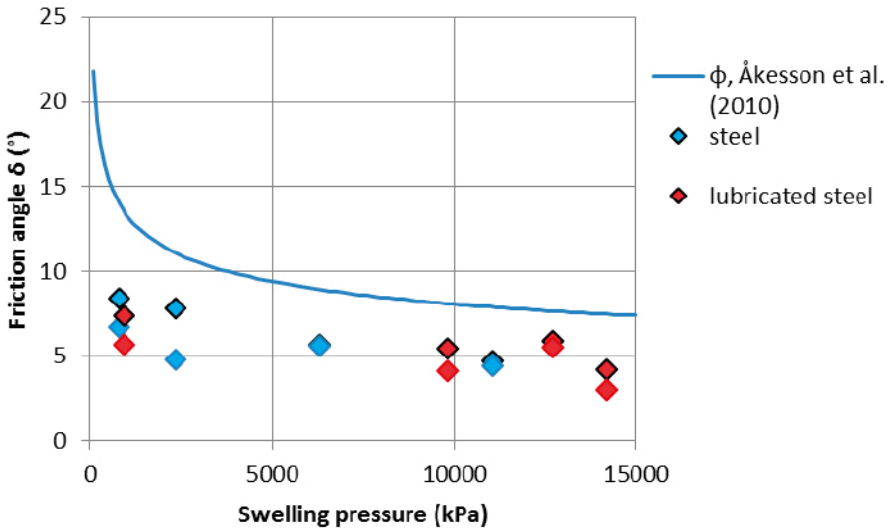

Figure 5-30. *Test results plotted with a relation used by Åkesson et al. (2010). For each test both a peak value, reached after the beginning of deformation (plotted with black marker lines) and a value reached after some deformation are shown.*

Observations

In general the main purpose of the report was to provide results that can be used for modelling, but the following observations could also be made:

- A peak value was seen in the friction force and the calculated friction angle δ at the first small deformation, i.e. less than 1 mm.
- No influence of deformation rate was seen on the friction angle.
- No effect of lubrication was seen in the evaluated friction angle.
- The friction angle δ seemed to have a value approximately equal to half of the bentonite friction angle $\phi/2$.

References

SKB's (Svensk Kärnbränslehantering AB) publications can be found at www.skb.se/publications.

Börgesson L, Johannesson L-E, Sandén T, Hernelind J, 1995. Modelling of the physical behaviour of water saturated clay barriers. Laboratory tests, material models and finite element application. SKB TR 95-20, Svensk Kärnbränslehantering AB.

Dueck A, Goudarzi R, Börgesson L, 2011. Buffer homogenisation, status report. SKB TR-12-02, Svensk Kärnbränslehantering AB.

Karnland O, Olsson S, Nilsson U, 2006. Mineralogy and sealing properties of various bentonites and smectite-rich clay material. SKB TR-06-30, Svensk Kärnbränslehantering AB.

Åkesson M, Börgesson L, Kristensson O, 2010. SR-Site Data report. THM modelling of buffer, backfill and other system components. SKB TR-10-44, Svensk Kärnbränslehantering AB.

Appendix 1

Swelling pressure development with time (basic series)

Swelling pressure, axially and radially measured stresses, development with time are given in diagrams for all tests. Dry densities and swelling are also given. Each series is presented in separate sections.

A1.1 Axial swelling

A01-12	Test description: Saturation and axial swelling						Final H (mm) 20.8 Final D (mm) 50
Date	**Height mm**	**Dry density kg/m³**	**Axial stress kPa**	**Radial stress kPa**	**Mean stress kPa**	**Swelling $\rho_{di}/\rho_{df}-1$ %**	**Remarks**
	20.0						compaction
2011-02-10	20.0		628	368	455		start
2011-02-22	20.0	1,659	9,629	12,600	11,610		saturation (i)
2011-02-22	20.8	1,659	1,579	3,165	2,636		
2011-03-07	20.9	1,564	5,976	8,436	7,616	6.0	final swelling (f)

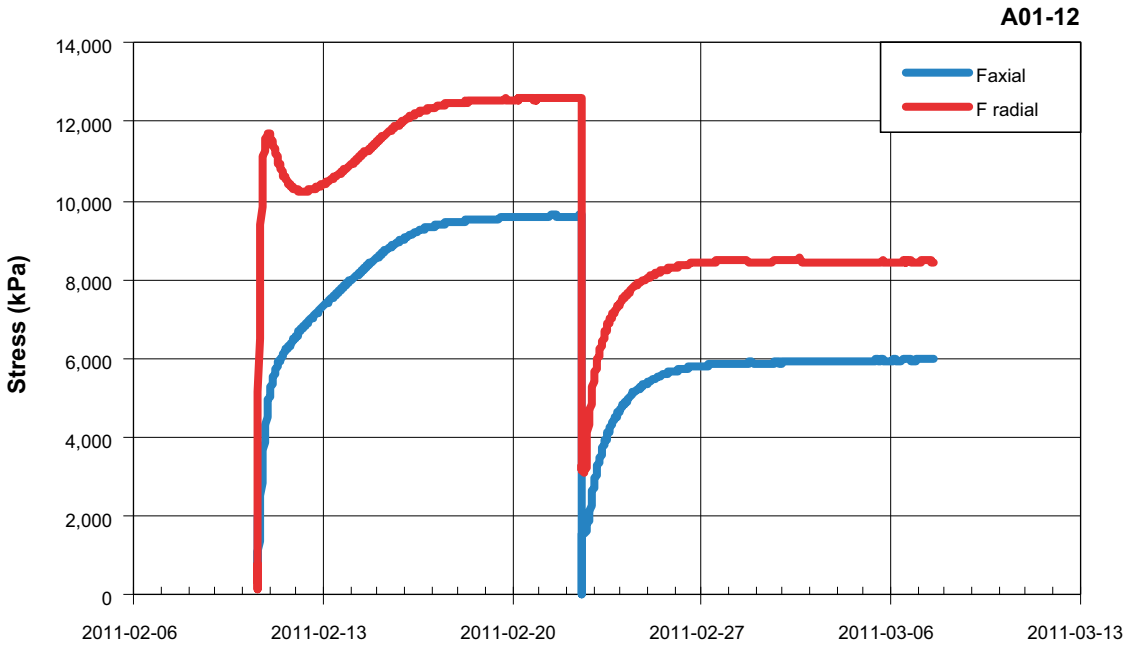

A01-13	Test description: Saturation and axial swelling						Final H (mm) 22.9 Final D (mm) 50
Date	**Height mm**	**Dry density kg/m³**	**Axial stress kPa**	**Radial stress kPa**	**Mean stress kPa**	**Swelling $\rho_{di}/\rho_{df}-1$ %**	**Remarks**
	20.0						compaction
2011-03-08	20.0		510	1,029	856		start
2011-03-23	20.0	1,655	8,604	9,994	9,531		saturation (i)
2011-03-23	22.8	1,655	685	1,832	1,450		
2011-04-07	22.9	1,425	2,566	3,240*	3,016	16.2	final swelling (f)

* corrected value.

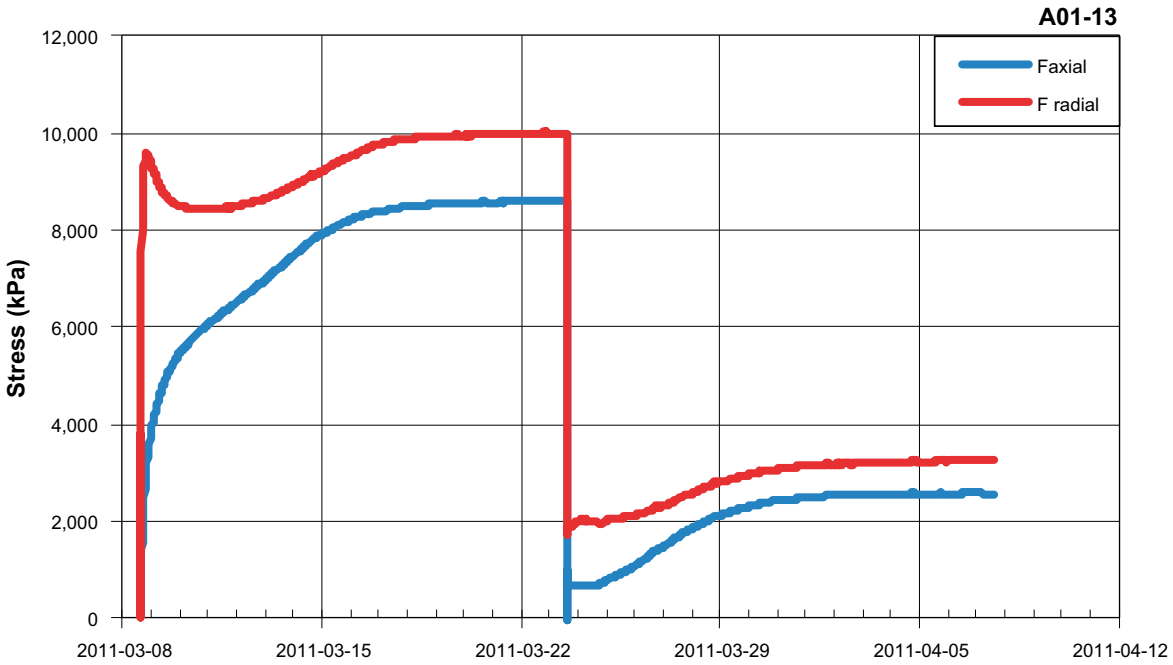

A1.2 Radial outward swelling

R11-17	Test description: Only radial outward swelling						Final H (mm) 40 Final D (mm) 46.8
Date	**Diameter mm**	**Dry density kg/m³**	**Axial stress kPa**	**Radial stress kPa**	**Mean stress kPa**	**Swelling $\rho_{di}/\rho_{df}-1$ %**	**Remarks**
		1,716*					compaction
2011-04-06	43.8	1,716	2,009	185	793	0.0	start swelling
2011-04-26	46.8	1,469	4,912	4,776	4,821	16.8	final swelling (f)

* approximate density.

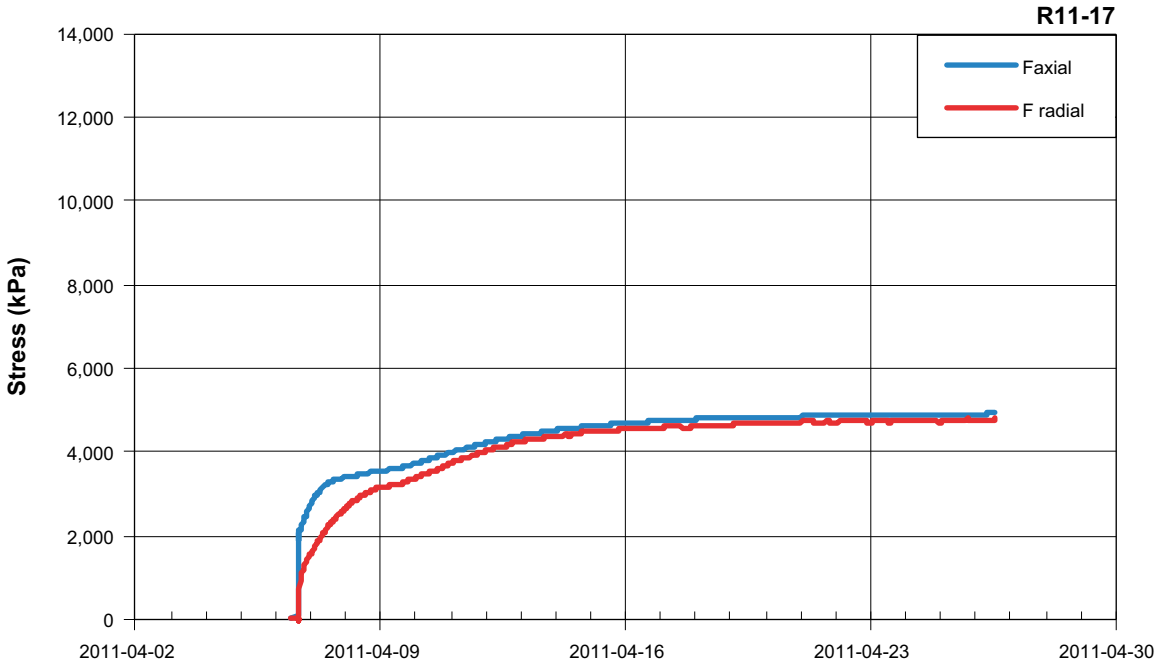

R11-18	Test description: Saturation and axial swelling						Final H (mm) 40 Final D (mm) 46.8
Date	**Height mm**	**Dry density kg/m³**	**Axial stress kPa**	**Radial stress kPa**	**Mean stress kPa**	**Swelling $\rho_{di}/\rho_{df}-1$ %**	**Remarks**
							compaction
2011-06-09			1,896	621	1,046		start
2011-06-20	46.8	1,655	11,979	9,926	10,611	0.0	saturation (i)
2011-06-20	43.8	1,655	1,339	175	563		start swelling
2011-07-05	46.9	1,402	3,077	2,683	2,814	18.0	final swelling (f)

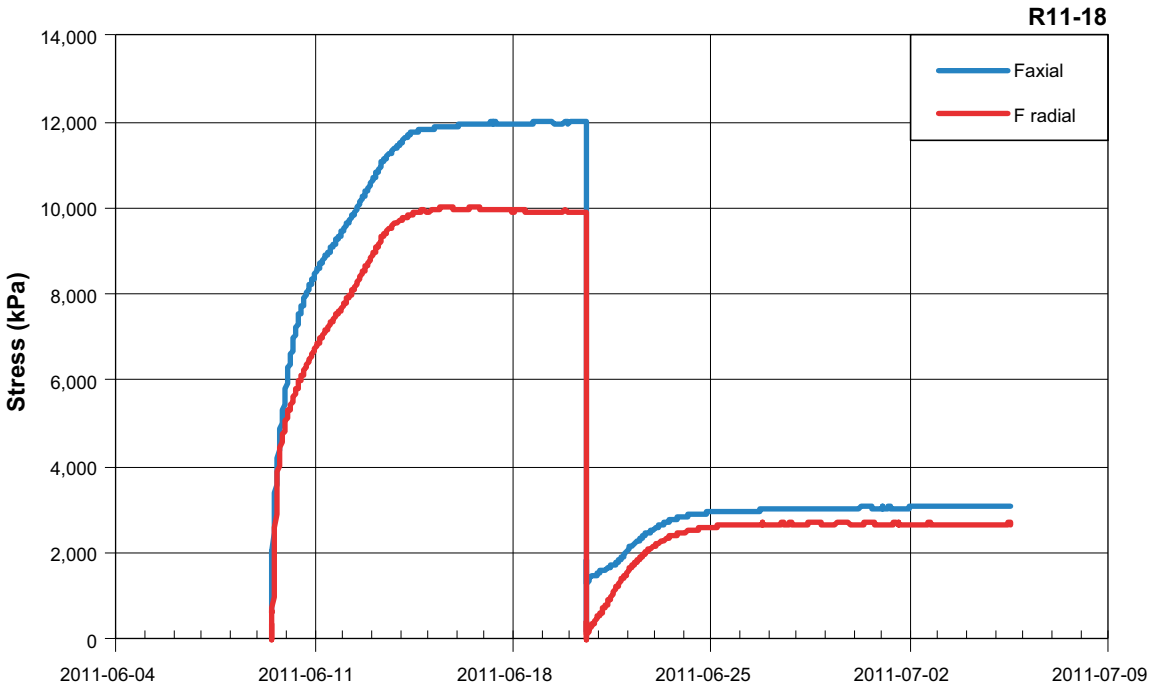

R11-19	Test description: Saturation and axial swelling						Final H (mm) 40 Final D (mm) 46.8
Date	**Height mm**	**Dry density kg/m³**	**Axial stress kPa**	**Radial stress kPa**	**Mean stress kPa**	**Swelling $\rho_{di}/\rho_{df}-1$ %**	**Remarks**
							compaction
2011-07-07			1,148	564	759		start
2011-07-19	46.8	1,656	12,857	10,565	11,329	0.0	saturation (i)
2011-07-19	40.8	1,656	394	149	231		start swelling
2011-08-04	46.9	1,256	383	182	249	31.8	final swelling (f)

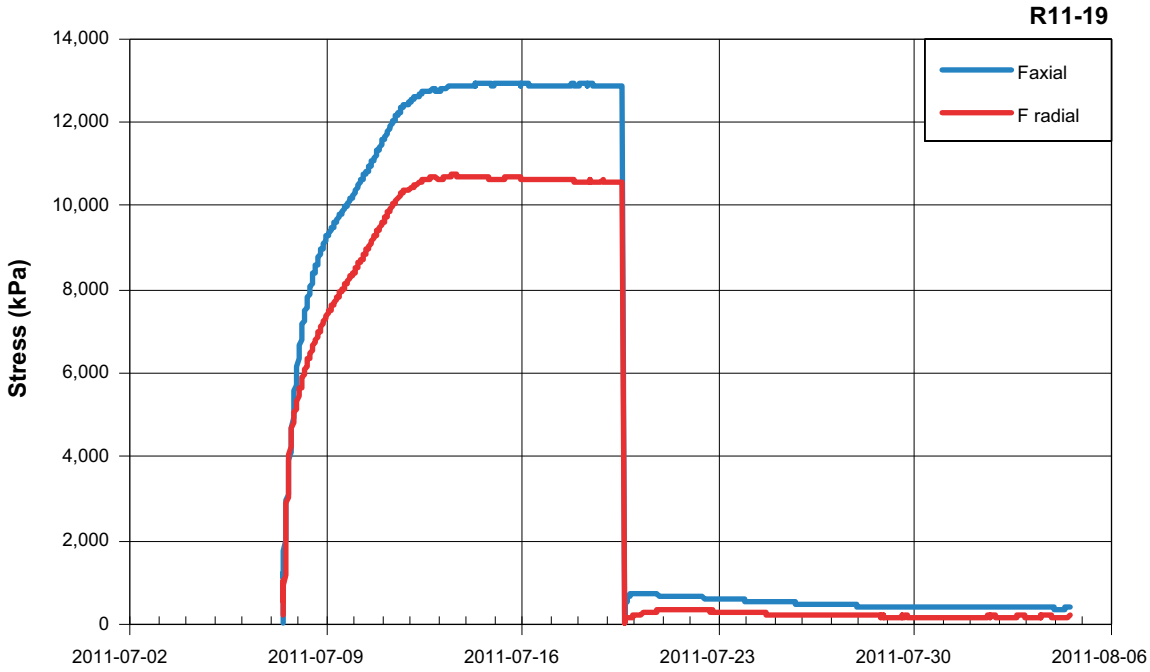

R11-20	Test description: Saturation and axial swelling						Final H (mm) 40 Final D (mm) 46.8
Date	**Height mm**	**Dry density kg/m³**	**Axial stress kPa**	**Radial stress kPa**	**Mean stress kPa**	**Swelling $\rho_{di}/\rho_{df}-1$ %**	**Remarks**
							compaction
2011-09-23			864	403	556		start
2011-10-05	46.8	1,655	12,756	11,270	11,765	0.0	saturation (i)
2011-10-05	40.8	1,655	235	143	174		start swelling
2011-10-19	46.9	1,258	843	930	901	31.6	final swelling (f)

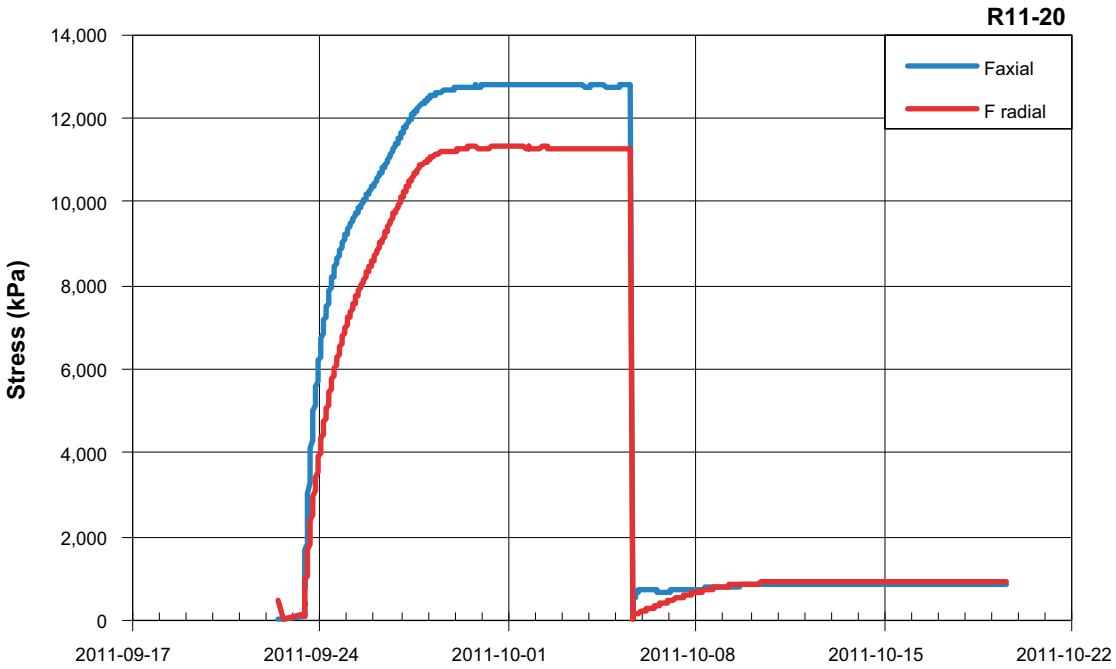

R11-21	Test description: Saturation and axial swelling						Final H (mm) 40 Final D (mm) 46.8
Date	**Height mm**	**Dry density kg/m³**	**Axial stress kPa**	**Radial stress kPa**	**Mean stress kPa**	**Swelling $\rho_{di}/\rho_{df}-1$ %**	**Remarks**
							compaction
2011-12-27		1,721	233	80	131		start
2011-01-10	46.8	1,721*	8,894	8,894	8,519	0.0	saturation (i)
2011-01-10	40.8	1,721*	222	136	165		start swelling
2011-01-31	46.8	1,317	314	230	258	30.6	final swelling (f)

* Uncertain density.

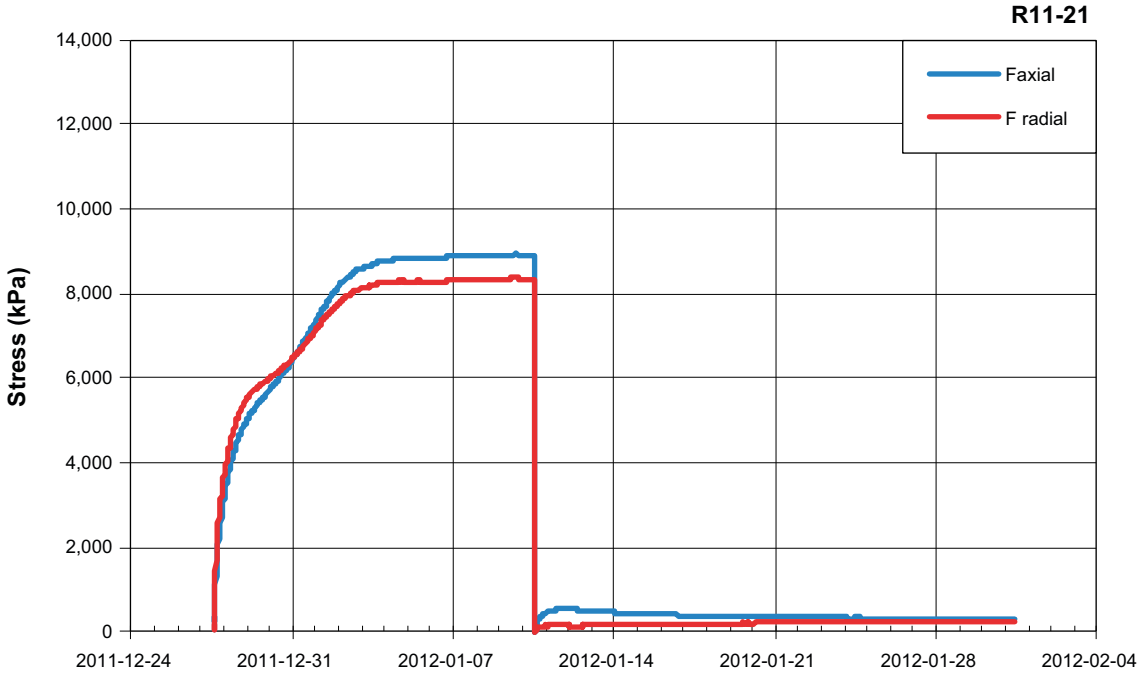

A1.3 Radial inward swelling

R21-9	Test description: Saturation and axial swelling						Final H (mm) 40 Final D (mm) 46.7
Date	**Diameter of cavity mm**	**Dry density kg/m³**	**Axial stress kPa**	**Radial stress kPa**	**Mean stress kPa**	**Swelling $\rho_{di}/\rho_{df}-1$ %**	**Remarks**
	0.0		0	0			compaction
2011-02-02 14:27	0.0		962	289	514		start
2011-02-14 13:30	0.0	1,655	12,537	9,863	10,754	0.0	saturation (i)
2011-02-14 15:11	10.5	1,655	6,875	5,016	5,636		
2011-02-28 16:30	0.0	1,558	7,093	6,497	6,696	6.2	final swelling (f)

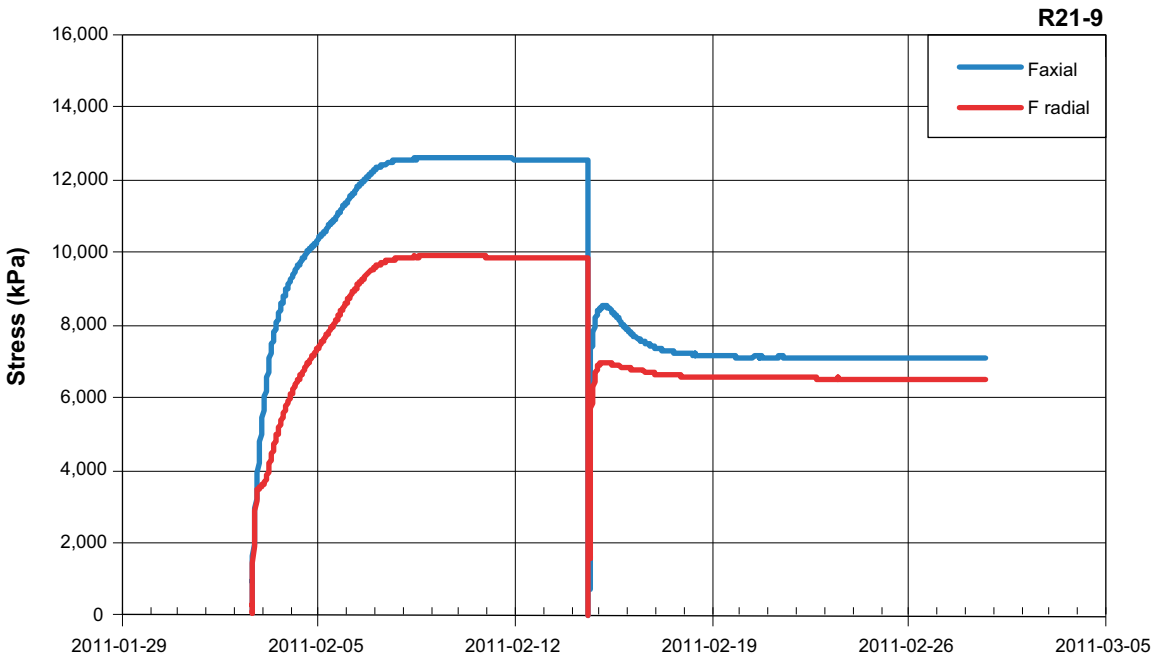

R21-10	Test description: Saturation and axial swelling						Final H (mm) 40 Final D (mm) 46.7
Date	**Diameter of cavity mm**	**Dry density kg/m³**	**Axial stress kPa**	**Radial stress kPa**	**Mean stress kPa**	**Swelling $\rho_{di}/\rho_{df}-1$ %**	**Remarks**
	0.0						compaction
2011-03-02 16:16	0.0		914	334	527		start
2011-03-14 15:15	0.0	1,656	12,369	13,818	13,335	0.0	saturation (i)
2011-03-14 16:07	19.0	1,656	3,502	1,998	2,500		
2011-03-29 14:00	0.0	1,346	2,468	1,692	1,951	23.0	final swelling (f)

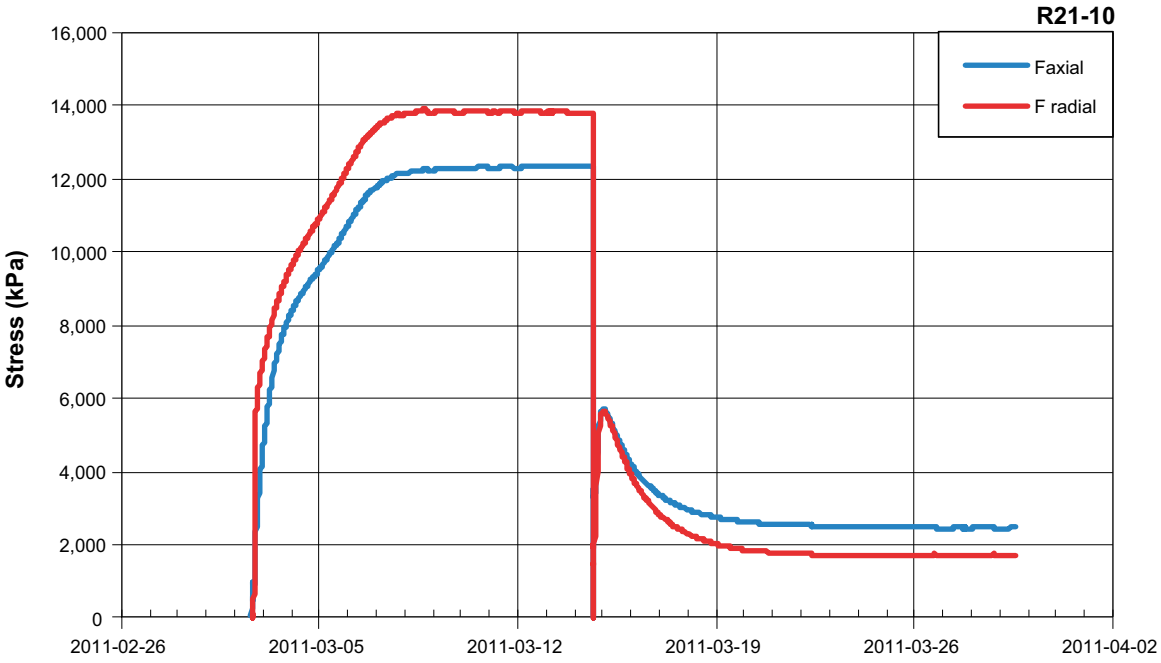

R21-11	Test description: Saturation and axial swelling						Final H (mm) 40 Final D (mm) 46.7
Date	**Diameter of cavity mm**	**Dry density kg/m³**	**Axial stress kPa**	**Radial stress kPa**	**Mean stress kPa**	**Swelling $\rho_{di}/\rho_{df}-1$ %**	**Remarks**
	0.0						compaction
2011-04-05 14:27	0.0		733	239	403		start
2011-04-18 12:30	0.0	1,657	12,569	11,355	11,759	0.0	saturation (i)
2011-04-18 14:00	8.0	1,657	998	5,308	3,871		
2011-05-03 10:30	0.0	1,596	8,303	7,590	7,828	3.8	final swelling (f)

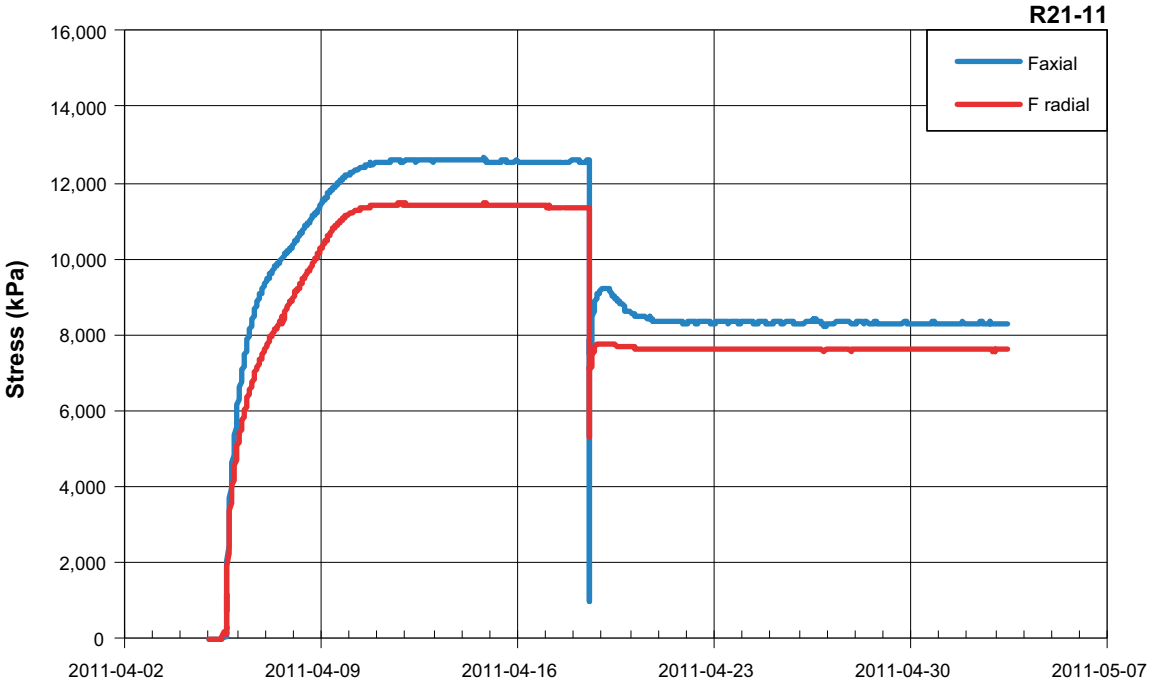

R21-12	Test description: Saturation and axial swelling						Final H (mm) 40 Final D (mm) 46.7
Date	**Diameter of cavity mm**	**Dry density kg/m³**	**Axial stress kPa**	**Radial stress kPa**	**Mean stress kPa**	**Swelling $\rho_{di}/\rho_{df}-1$ %**	**Remarks**
	0.0						compaction
2011-05-16 16:25	0.0		680	126	311		start
2011-05-27 13:00	0.0	1,660	11,968	10,104	10,725	0.0	saturation (i)
2011-05-27 14:03	23.0	1,660	3,263	1,309	1,960		
2011-06-07 14:00	0.0	1,265	1,802	1,477	1,585	31.2	final swelling (f)

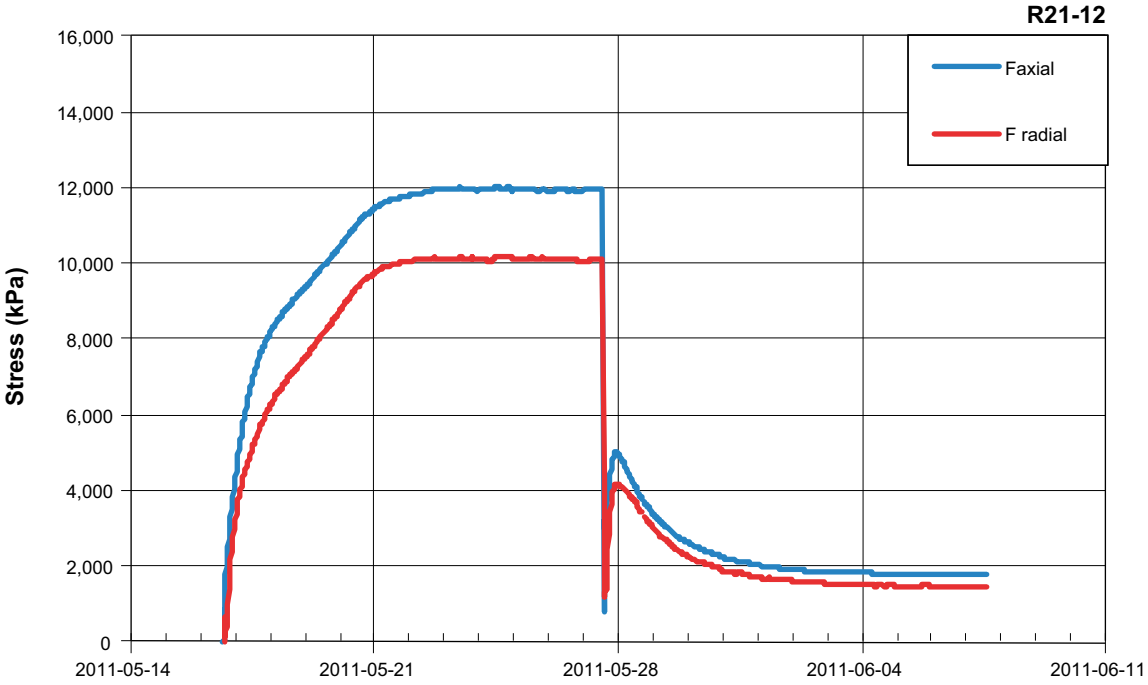

Appendix 2

Distribution of basic variables in the direction of swelling (basic series)

The distribution of the basic variables water content w, bulk density ρ, void ratio, dry density ρ_d and degree of saturation S_r, over the specimens in the swelling direction are given for all tests.

Table A2-1. Axial swelling. Distribution of basic variables over the specimen height.

A01-12								
from bottom mm	**thickness mm**	ρ_s **kg/m³**	ρ_w **kg/m³**	**W %**	ρ **kg/m³**	ρ_d **kg/m³**	**e**	S_r **%**
2.5	5	2,780	1,000	26.3	2,004	1,587	0.75	97
7.5	5	2,780	1,000	26.6	2,012	1,588	0.75	99
12.5	5	2,780	1,000	27.3	2,005	1,575	0.77	99
17.5	5	2,780	1,000	30.2	1,961	1,506	0.85	99
	average			27.6	1,995	1,564	0.78	99

A01-13								
from bottom mm	**thickness mm**	ρ_s **kg/m³**	ρ_w **kg/m³**	**W %**	ρ **kg/m³**	ρ_d **kg/m³**	**e**	S_r **%**
2.5	5	2,780	1,000	32.0	1,934	1,466	0.90	99
7.5	5	2,780	1,000	32.6	1,928	1,454	0.91	99
12.5	5	2,780	1,000	33.2	1,901	1,427	0.95	97
17.5	5	2,780	1,000	37.4	1,859	1,353	1.05	99
	average			33.8	1,906	1,425	0.95	99

Table A2-2. Radial outward swelling. Distribution of basic variables over the radius.

R11-17								
radius mm	**thickness mm**	ρ_s **kg/m³**	ρ_w **kg/m³**	**W %**	ρ **kg/m³**	ρ_d **kg/m³**	**e**	S_r **%**
4	8	2,780	1,000	29.1	1,964	1,521	0.83	98
12	8	2,780	1,000	30.3	1,960	1,504	0.85	99
20	8	2,780	1,000	33.0	1,912	1,438	0.93	98
	average			31.6	1,934	1,469	0.89	99

R11-18								
radius mm	**thickness mm**	ρ_s **kg/m³**	ρ_w **kg/m³**	**W %**	ρ **kg/m³**	ρ_d **kg/m³**	**e**	S_r **%**
4	8	2,780	1,000	31.9	1,937	1,469	0.89	98
12	8	2,780	1,000	32.8	1,924	1,448	0.92	99
20	8	2,780	1,000	37.4	1,870	1,361	1.04	100
	average			35.2	1,895	1,402	0.98	99

R11-19								
radius mm	**thickness mm**	ρ_s **kg/m³**	ρ_w **kg/m³**	**W %**	ρ **kg/m³**	ρ_d **kg/m³**	**e**	S_r **%**
4	8	2,780	1,000	39.9	1,837	1,313	1.12	99
12	8	2,780	1,000	40.3	1,823	1,300	1.14	98
20	8	2,780	1,000	47.5	1,797	1,361	1.28	103
	average			44.2	1,810	1,219	1.28	101

R11-20								
radius mm	**thickness mm**	ρ_s **kg/m³**	ρ_w **kg/m³**	**W %**	ρ **kg/m³**	ρ_d **kg/m³**	**e**	S_r **%**
4	8	2,780	1,000	43.8	1,807	1,257	1.21	100
12	8	2,780	1,000	42.9	1,800	1,260	1.21	99
20	8	2,780	1,000	42.9	1,797	1,257	1.21	99
	average			43.0	1,799	1,258	1.21	99

R11-21								
radius mm	**thickness mm**	ρ_s **kg/m³**	ρ_w **kg/m³**	**W %**	ρ **kg/m³**	ρ_d **kg/m³**	**e**	S_r **%**
4	8	2,780	1,000	38.6	1,859	1,341	1.07	100
12	8	2,780	1,000	39.2	1,851	1,330	1.09	100
20	8	2,780	1,000	42.1	1,855	1,305	1.13	104
	average			40.7	1,854	1,317	1.1	102

Table A2-3. Radial inward swelling. Distribution of basic variables over the radius.

R21-9								
radius mm	**thickness mm**	ρ_s **kg/m³**	ρ_w **kg/m³**	**W %**	ρ **kg/m³**	ρ_d **kg/m³**	**e**	S_r **%**
4	8	2,780	1,000	31.0	1,933	1,476	0.88	97
12	8	2,780	1,000	27.6	2,002	1,569	0.77	99
20	8	2,780	1,000	27.5	2,000	1,568	0.77	99
	average			27.9	1,993	1,558	0.8	99

R21-10								
radius mm	**thickness mm**	ρ_s **kg/m³**	ρ_w **kg/m³**	**W %**	ρ **kg/m³**	ρ_d **kg/m³**	**e**	S_r **%**
4	8	2,780	1,000	48.4	1,828	1,231	1.26	107
12	8	2,780	1,000	41.2	1,880	1,331	1.09	105
20	8	2,780	1,000	37.9	1,900	1,378	1.02	104
	average			40.2	1,885	1,346	1.1	104*

* uncertain.

R21-11								
radius mm	**thickness mm**	ρ_s **kg/m³**	ρ_w **kg/m³**	**W %**	ρ **kg/m³**	ρ_d **kg/m³**	**e**	S_r **%**
4	8	2,780	1,000	27.8	1,974	1,545	0.80	97
12	8	2,780	1,000	25.5	2,026	1,614	0.72	98
20	8	2,780	1,000	26.4	2,017	1,596	0.74	99
	average			26.2	2,015	1,596	0.7	98

R21-12								
radius mm	**thickness mm**	ρ_s **kg/m³**	ρ_w **kg/m³**	**W %**	ρ **kg/m³**	ρ_d **kg/m³**	**e**	S_r **%**
4	8	2,780	1,000	54.0	1,531	994	1.80	84
12	8	2,780	1,000	45.0	1,835	1,265	1.20	105
20	8	2,780	1,000	40.3	1,852	1,319	1.11	101
	average			43.4	1,810	1,265	1.2	100

Appendix 3

Final values of basic variables and swelling pressure (basic series)

In the tables the final values of the basic variables (water content w, bulk density ρ, dry density ρ_d, degree of saturation S_r) and the swelling pressure (axial stress P_a, radial stress P_r) are given. The last column contains the total time for each test divided into the time for saturation t_1 and the time for homogenisation t_2 ($t_1 + t_2$).

Table A3-1. Axial swelling. Results from series A01.

	Swelling		Average over specimen				Swelling pressure		Total time
Sample ID	Swelling phase 2 %	$\rho_{di}/\rho_{df}-1$ %	w %	ρ kg/m³	ρ_{df} kg/m³	S_r %	Axial P_a kPa	Radial P_r kPa	days
A01-12	4	6	27.6	1,995	1,564	99	5,976	8,436	12 + 13
A01-13	14	16	33.8	1,906	1,425	99	2,566	3,240	15 + 16

Table A3-2. Radial outward swelling. Results from series R11.

	Swelling		Average over specimen height				Swelling pressure		Total time
Sample ID	Swelling phase 2 %	$\rho_{di}/\rho_{df}-1$ %	w %	ρ kg/m³	ρ_{df} kg/m³	S_r %	Axial P_a kPa	Radial P_r kPa	days
R11-17	14	17	31.6	1,934	1,469	99	4,912	4,776	0 + 20
R11-18	14	18	35.2	1,895	1,402	99	3,077	2,683	11 + 15
R11-19	32	32	44.2	1,810	1,256	101	383	182	12 + 16
R11-20	32	32	43.0	1,799	1,258	99	843	930	12 + 14
R11-21	32	31	40.7	1,854	1,317	102	314	230	14 + 21

Table A3-3. Radial inward swelling. Results from series R21.

	Swelling		Average over specimen				Swelling pressure		Total time
Sample ID	Swelling phase 2 %	$\rho_{di}/\rho_{df}-1$ %	w %	ρ kg/m³	ρ_{df} kg/m³	S_r %	Axial P_a kPa	Radial P_r kPa	days
R21-9	5	6	27.9	1,993	1,558	99	7,093	6,497	12 + 14
R21-10	20	23	40.2	1,885	1,346	104	2,468	1,692	12 + 15
R21-11	3	4	26.2	2,015	1,596	98	8,303	7,590	13 + 15
R21-12	32	31	43.4	1,810	1,265	100	1,802	1,477	11 + 11

Appendix 4

Final values of basic variables and swelling pressure (high resolution)

In the tables the final values of the basic variables (water content w, bulk density ρ, dry density ρ_d, degree of saturation S_r) and the swelling pressure (axial stress P_a, radial stress P_r) are given. The last column contains the total time for each test divided into the time for saturation t_1 and the time for homogenisation t_2 ($t_1 + t_2$). In the table the position 1, 2, 3 and 4 means 15 mm, 30 mm, 45 and 60 mm, respectively from bottom surface of the specimen and the abbreviation avr. means average over the specimen.

Table A4-1. Results from high resolution series and tests HR-Ro1 and HR-A1.

	Swelling			Average over specimen height/radius				Swelling pressure		Total time
Sample ID	Swelling phase 2 %	$\rho_{di}/\rho_{df}-1$ %	pos.	w %	ρ kg/m^3	ρ_{df} kg/m^3	S_r %	Axial P_a kPa	Radial P_r kPa	days
HR-Ro1	43	42	avr.	50.3	1,754	1,171	101	550	435	0 + 49
			1	50.0	1,756	1,174	101		437	
			2	50.0	1,757	1,175	101		477	
			3	50.4	1,754	1,170	101		364	
			4	50.9	1,749	1,164	101		463	
HR-A1	26	32	avr.	43.6	1,801	1,258	99	789	1,016	0 + 67
			1	40.2	1,829	1,304	99		1,280	
			2	41.9	1,804	1,272	98		1,056	
			3	54.4	1,700	1,104	99		712	

Appendix 5

Measurements of friction between buffer and other surfaces

Test results presented as the time evolution of swelling pressure (axial and radial stresses) and the evaluated friction angel as a function of deformation.

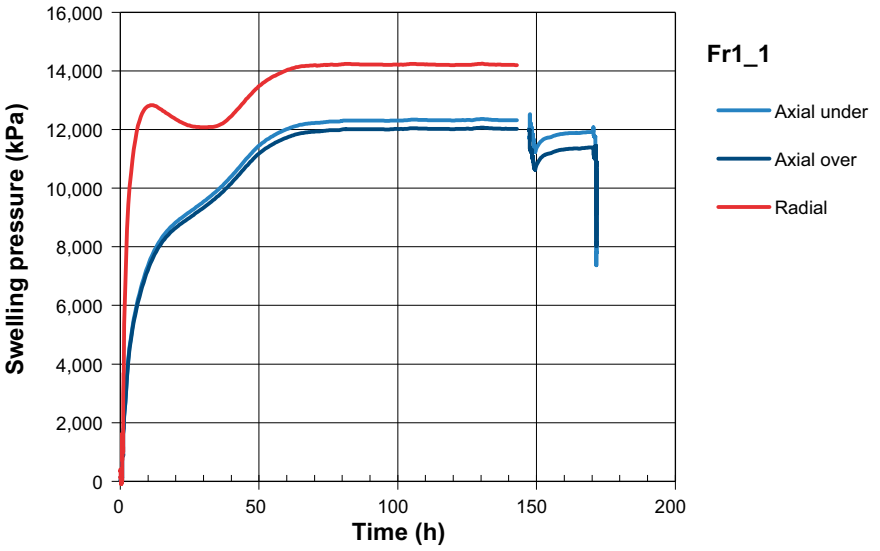

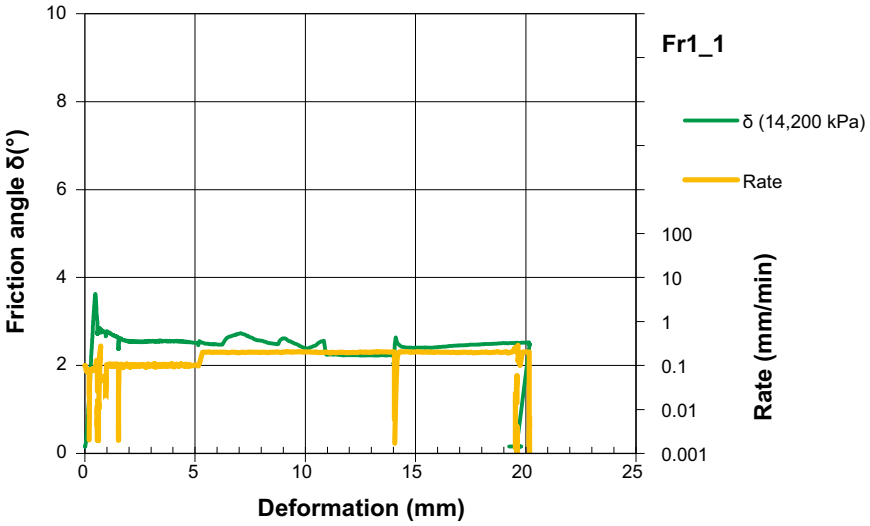

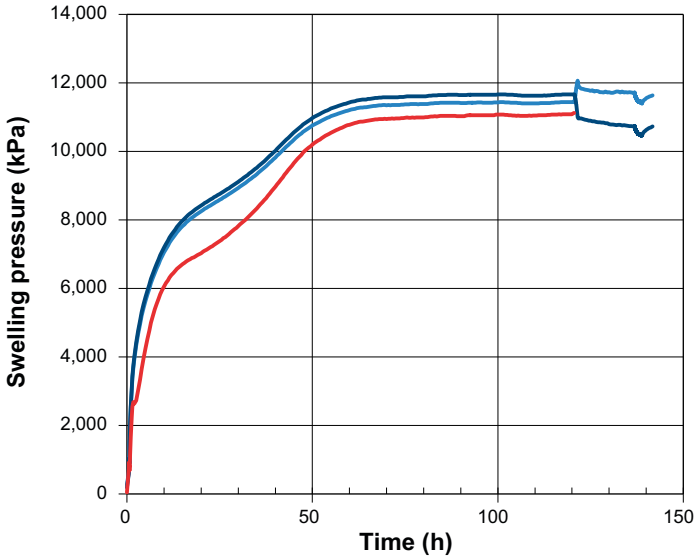
Fr1_2
Axial under
Axial over
Radial
Swelling pressure (kPa)
Time (h)
14,000
12,000
10,000
8,000
6,000
4,000
2,000
0
0
50
100
150

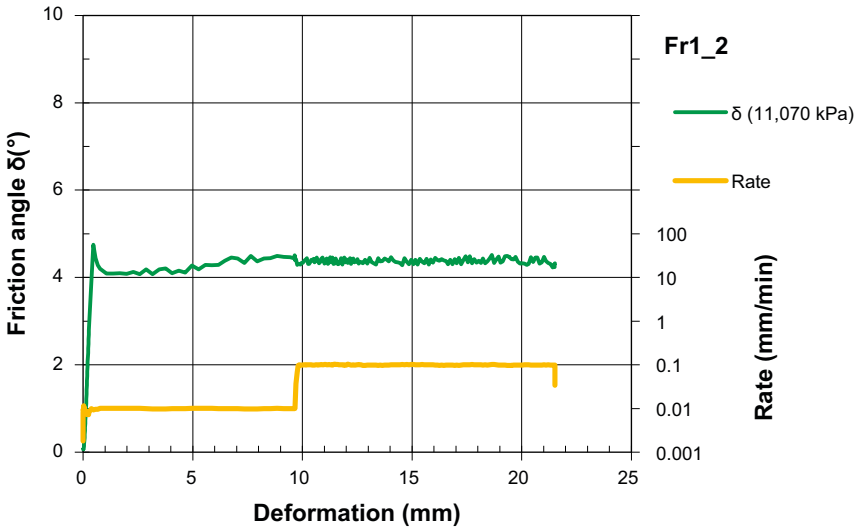
Fr1_2
δ (11,070 kPa)
Rate
Friction angle δ(°)
Rate (mm/min)
Deformation (mm)
10
8
6
4
2
0
100
10
1
0.1
0.01
0.001
0
5
10
15
20
25

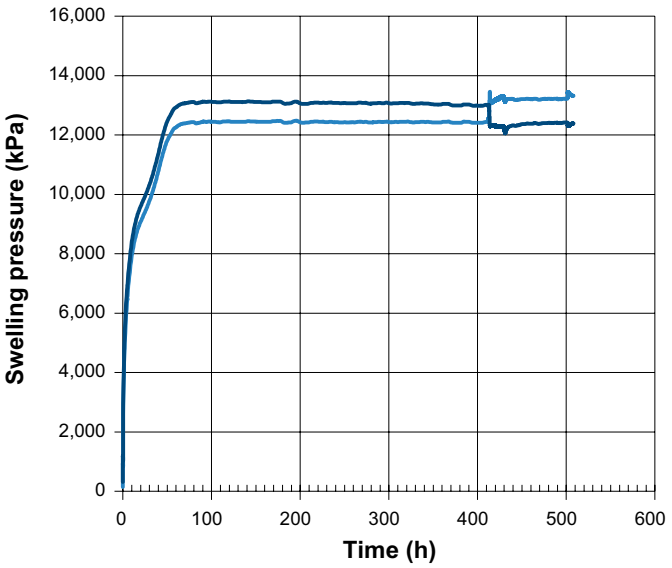
Fr1_3
Axial under
Axial over
Swelling pressure (kPa)
Time (h)
16,000
14,000
12,000
10,000
8,000
6,000
4,000
2,000
0
0
100
200
300
400
500
600

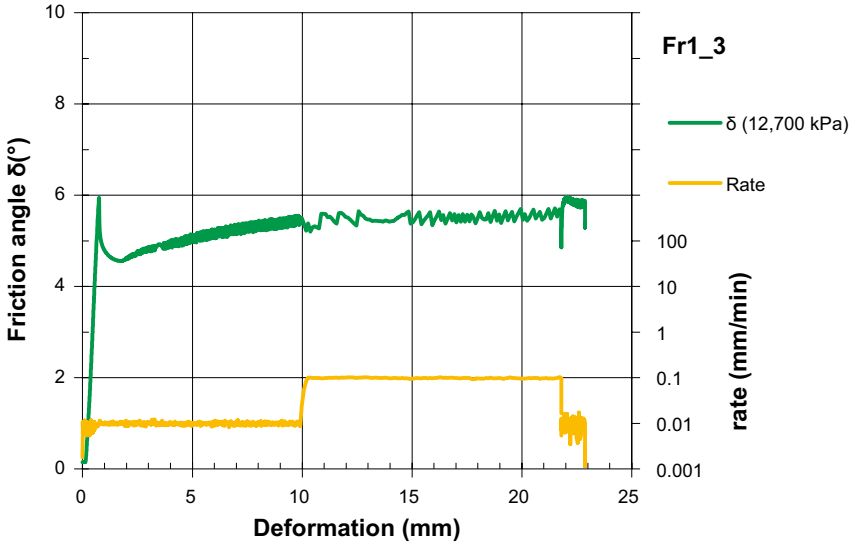
Fr1_3
δ (12,700 kPa)
Rate
Friction angle δ(°)
rate (mm/min)
Deformation (mm)
10
8
6
4
2
0
100
10
1
0.1
0.01
0.001
0
5
10
15
20
25

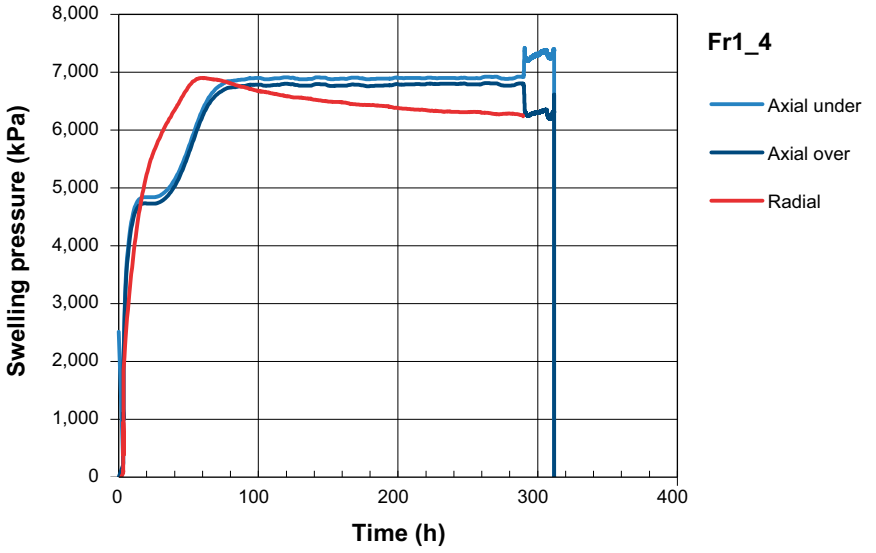
Fr1_4
Axial under
Axial over
Radial
Swelling pressure (kPa)
Time (h)
8,000
7,000
6,000
5,000
4,000
3,000
2,000
1,000
0
0
100
200
300
400

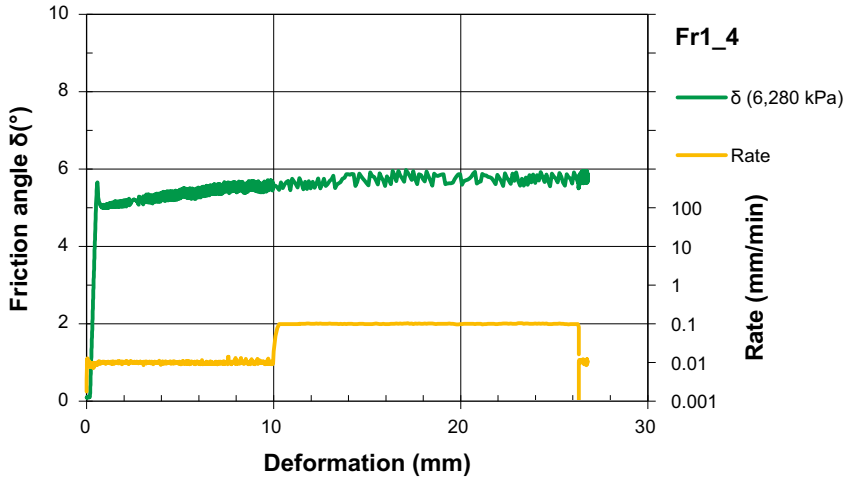
Fr1_4
δ (6,280 kPa)
Rate
Friction angle δ(°)
Rate (mm/min)
Deformation (mm)
10
8
6
4
2
0
100
10
1
0.1
0.01
0.001
0
10
20
30

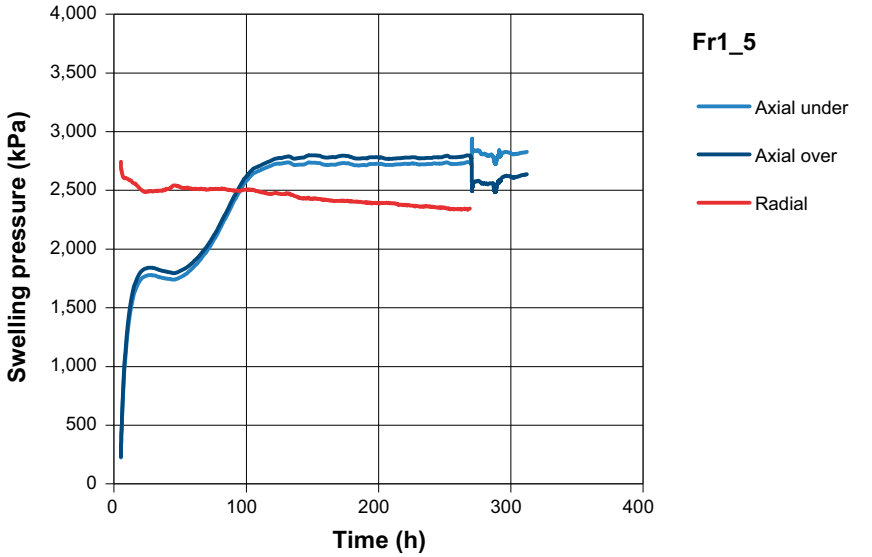
Fr1_5
Axial under
Axial over
Radial
Swelling pressure (kPa)
Time (h)
4,000
3,500
3,000
2,500
2,000
1,500
1,000
500
0
0
100
200
300
400

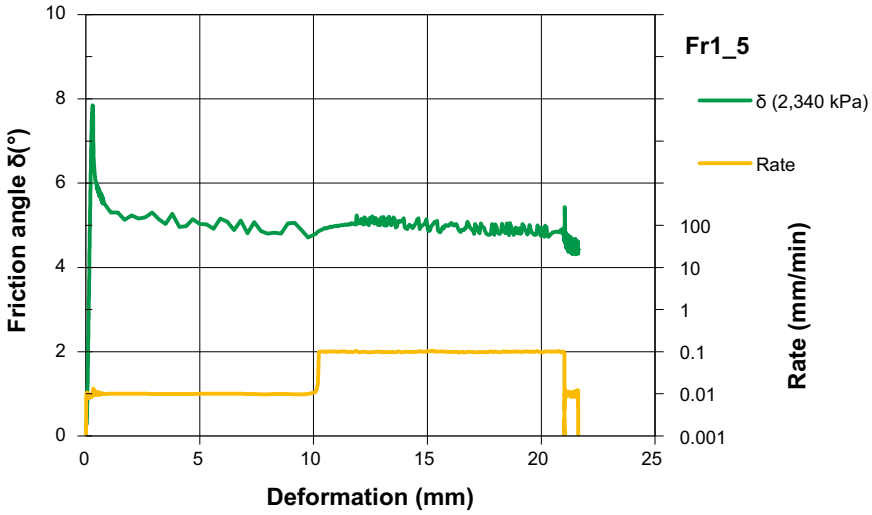
Fr1_5
δ (2,340 kPa)
Rate
Friction angle δ(°)
Rate (mm/min)
Deformation (mm)
10
8
6
4
2
0
0
5
10
15
20
25
100
10
1
0.1
0.01
0.001

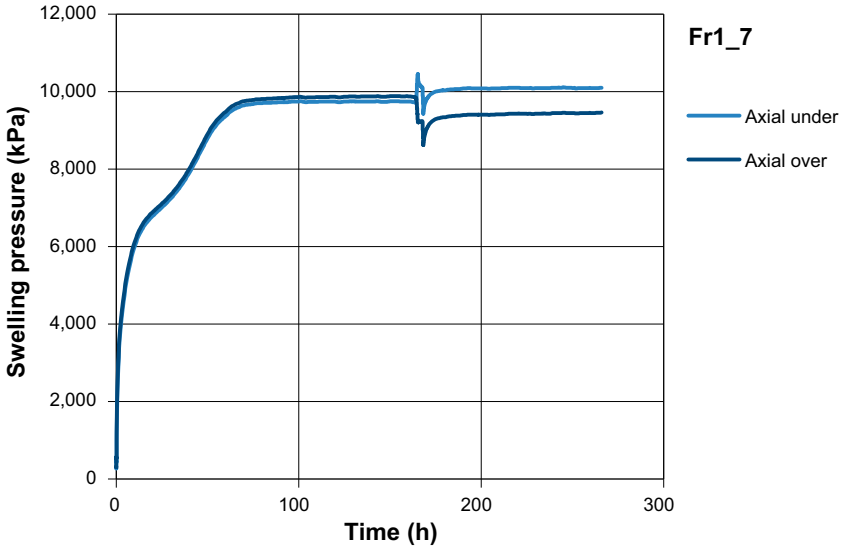
Fr1_7
Axial under
Axial over
Swelling pressure (kPa)
Time (h)
12,000
10,000
8,000
6,000
4,000
2,000
0
0
100
200
300

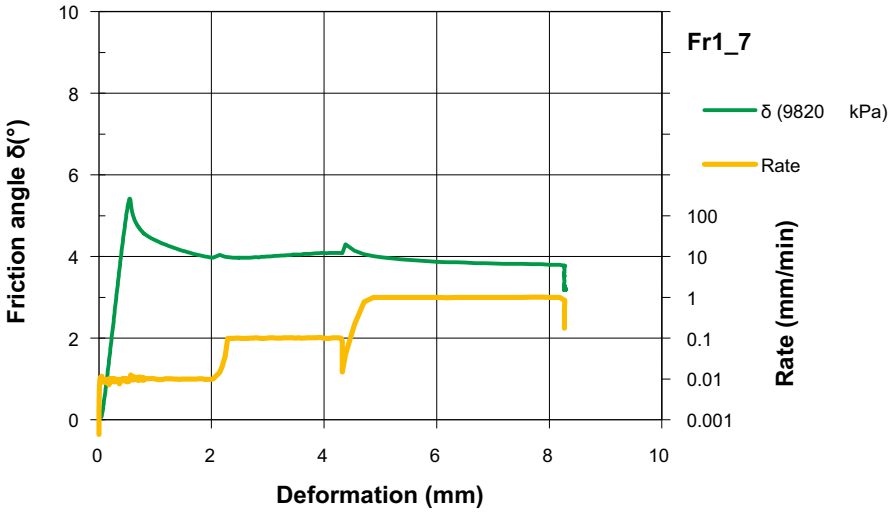
Fr1_7
δ (9820 kPa)
Rate
Friction angle δ(°)
Rate (mm/min)
Deformation (mm)
10
8
6
4
2
0
100
10
1
0.1
0.01
0.001
0
2
4
6
8
10

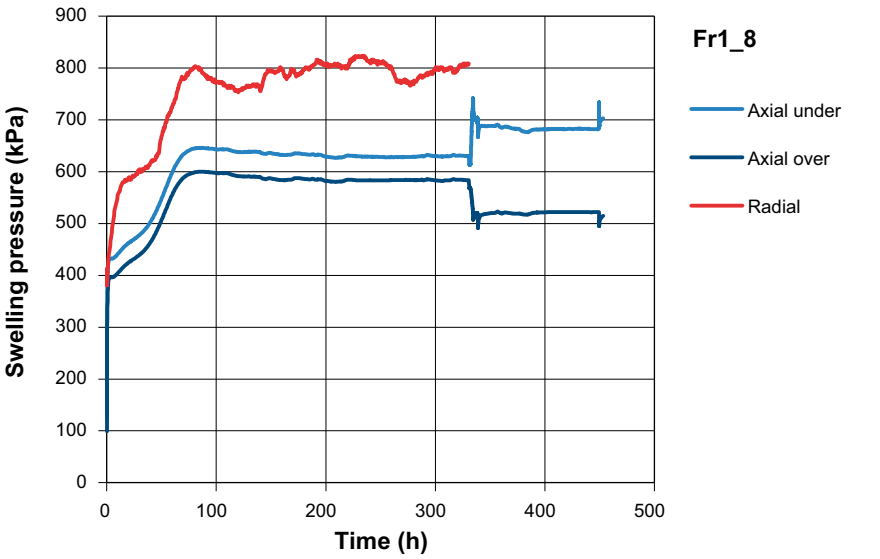
Fr1_8
Axial under
Axial over
Radial
Swelling pressure (kPa)
Time (h)
900
800
700
600
500
400
300
200
100
0
0
100
200
300
400
500

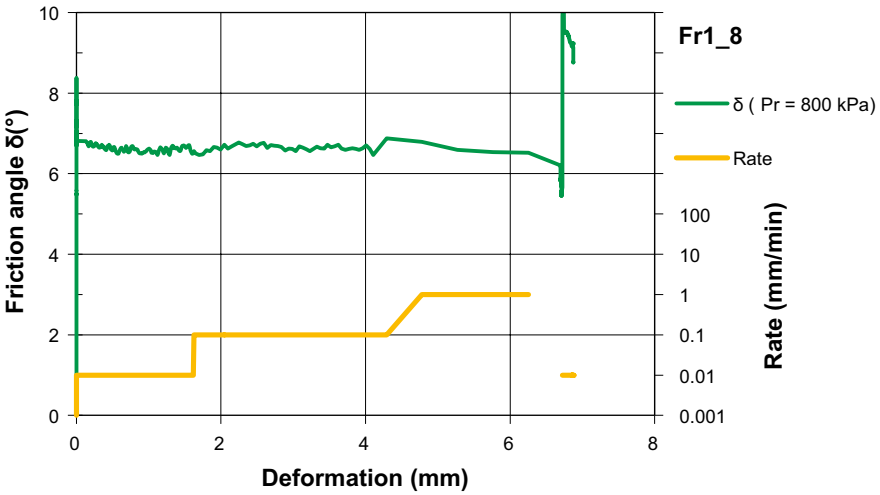
Fr1_8
δ (Pr = 800 kPa)
Rate
Friction angle δ(°)
Rate (mm/min)
Deformation (mm)
10
8
6
4
2
0
100
10
1
0.1
0.01
0.001
0
2
4
6
8

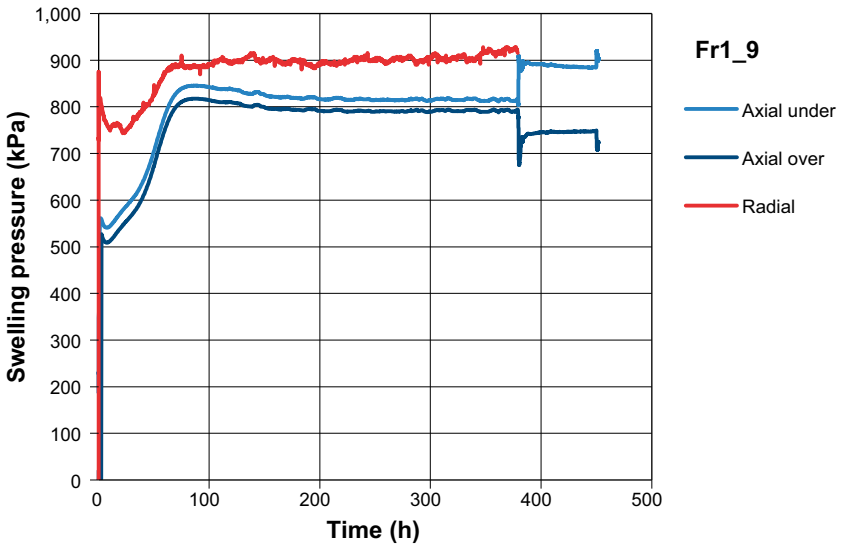
Fr1_9
Axial under
Axial over
Radial
Swelling pressure (kPa)
Time (h)
1,000
900
800
700
600
500
400
300
200
100
0
0
100
200
300
400
500

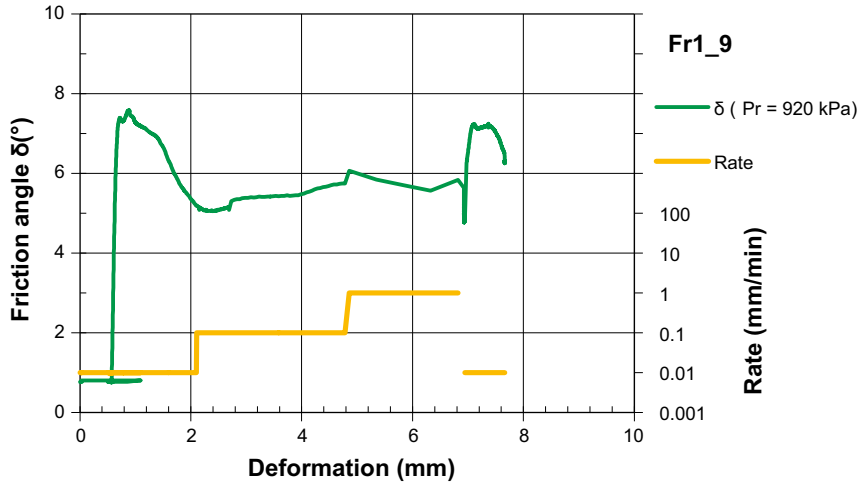
Fr1_9
δ (Pr = 920 kPa)
Rate
Friction angle δ(°)
Rate (mm/min)
Deformation (mm)
10
8
6
4
2
0
0
2
4
6
8
10
100
10
1
0.1
0.01
0.001